

# Chapter 7

## Materials Characterization

### 7.1 Rutherford Backscattering of Thin Films<sup>1</sup>

#### 7.1.1 Introduction

One of the main research interests of the semiconductor industry is to improve the performance of semi-conducting devices and to construct new materials with reduced size or thickness that have potential application in transistors and microelectronic devices. However, the most significant challenge regarding thin film semiconductor materials is measurement. Properties such as the thickness, composition at the surface, and contamination, all are critical parameters of the thin films. To address these issues, we need an analytical technique which can measure accurately through the depth of the of the semiconductor surface without destruction of the material. Rutherford backscattering spectroscopy is a unique analysis method for this purpose. It can give us information regarding in-depth profiling in a non-destructive manner. However X-ray photo electron spectroscopy (XPS), energy dispersive X-ray analysis (EDX) and Auger electron spectroscopy are also able to study the depth-profile of semiconductor films. Table 7.1 demonstrates the comparison between those techniques with RBS.

Method	Destructive	Incident particle	Outgoing Particle	Detection limit	Depth resolution
RBS	No	Ion	Ion	~1	10 nm
XPS	Yes	X-ray photon	Electron	~0.1-1	~1 $\mu\text{m}$
EDX	Yes	Electron	X-ray photon	~0.1	1.5 nm
Auger	Yes	Electron	Electron	~0.1-1	1.5 nm

**Table 7.1:** Comparison between different thin film analysis techniques.

#### 7.1.2 Basic concept of Rutherford backscattering spectroscopy

At a basic level, RBS demonstrates the electrostatic repulsion between high energy incident ions and target nuclei. The specimen under study is bombarded with monoenergetic beam of  $^4\text{He}^+$  particles and the backscattered particles are detected by the detector-analysis system which measures the energies of the particles. During the collision, energy is transferred from the incident particle to the target specimen atoms; the change in energy of the scattered particle depends on the masses of incoming and target atoms. For an

<sup>1</sup>This content is available online at <<http://cnx.org/content/m22411/1.3/>>.

incident particle of mass  $M_1$ , the energy is  $E_0$  while the mass of the target atom is  $M_2$ . After the collision, the residual energy  $E$  of the particle scattered at angle  $\emptyset$  can be expressed as:

$$E = k^2 E_0$$

$$k = \frac{\left( M_1 \cos \emptyset + \sqrt{M_2^2 - M_1^2 \sin^2 \emptyset} \right)}{M_1 + M_2}$$

where  $k$  is the kinematic scattering factor, which is actually the energy ratio of the particle before and after the collision. Since  $k$  depends on the masses of the incident particle and target atom and the scattering angle, the energy of the scattered particle is also determined by these three parameters. A simplified layout of backscattering experiment is shown in Figure 1 (Figure 7.1).

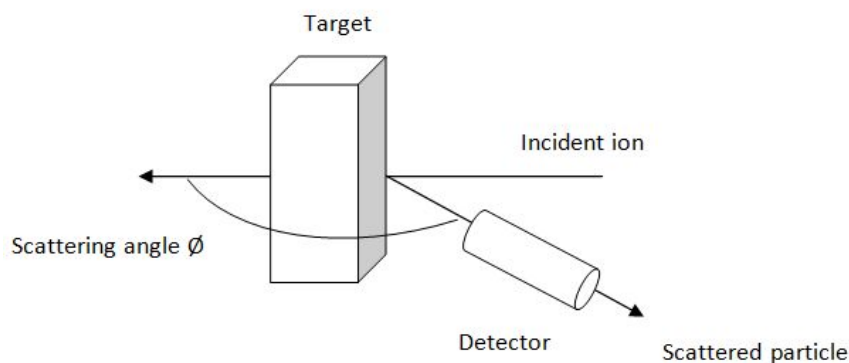


**Figure 7.1:** Schematic representation of the experimental setup for Rutherford backscattering analysis.

The probability of a scattering event can be described by the differential scattering cross section of a target atom for scattering an incoming particle through the angle  $\emptyset$  into differential solid angle as follows,

$$\frac{d\sigma_R}{d\phi} = \left( \frac{zZe^2}{2E_0 \sin^2 \emptyset} \right) \frac{\left[ \cos \emptyset + \sqrt{1 - \left( \frac{M_1}{M_2} \sin \emptyset \right)^2} \right]^2}{\sqrt{1 - \left( \frac{M_1}{M_2} \sin \emptyset \right)^2}}$$

where  $d\sigma_R$  is the effective differential cross section for the scattering of a particle. The above equation may look complicated but it conveys the message that the probability of scattering event can be expressed as a function of scattering cross section which is proportional to the  $zZ$  when a particle with charge  $ze$  approaches the target atom with charge  $Ze$ .

Helium ions not scattered at the surface lose energy as they traverse the solid. They lose energy due to interaction with electrons in the target. After collision the He particles lose further energy on their way out to the detector. We need to know two quantities to measure the energy loss, the distance  $\Delta t$  that the particles penetrate into the target and the energy loss  $\Delta E$  in this distance Figure 7.2. The rate of energy loss

or stopping power is a critical component in backscattering experiments as it determines the depth profile in a given experiment.

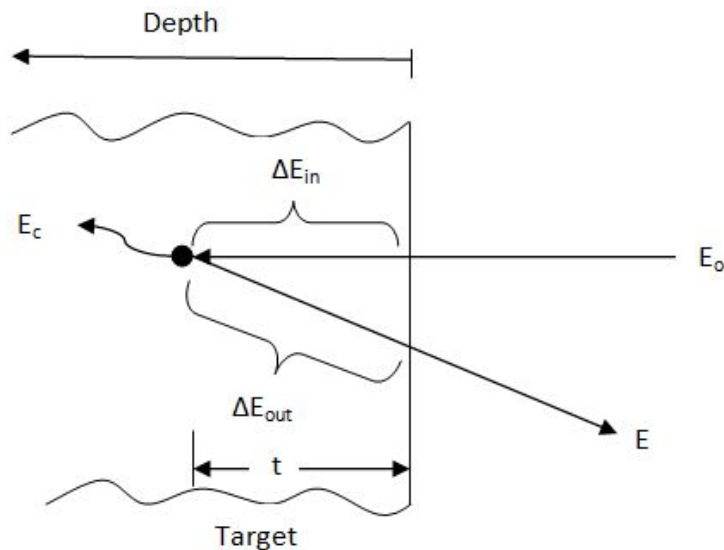


**Figure 7.2:** Components of energy loss for a ion beam that scatters from depth  $t$ . First, incident beam loses energy through interaction with electrons  $\Delta E_{in}$ . Then energy lost occurs due to scattering  $E_c$ . Finally outgoing beam loses energy for interaction with electrons  $\Delta E_{out}$ . Adapted from L. C. Feldman and J. W. Mayer, *Fundamentals of Surface and Thin Film Analysis*, North Holland-Elsevier, New York (1986).

In thin film analysis, it is convenient to assume that total energy loss  $\Delta E$  into depth  $t$  is only proportional to  $t$  for a given target. This assumption allows a simple derivation of energy loss in backscattering as more complete analysis requires many numerical techniques. In constant  $dE/dx$  approximation, total energy loss becomes linearly related to depth  $t$ , Figure 7.3.

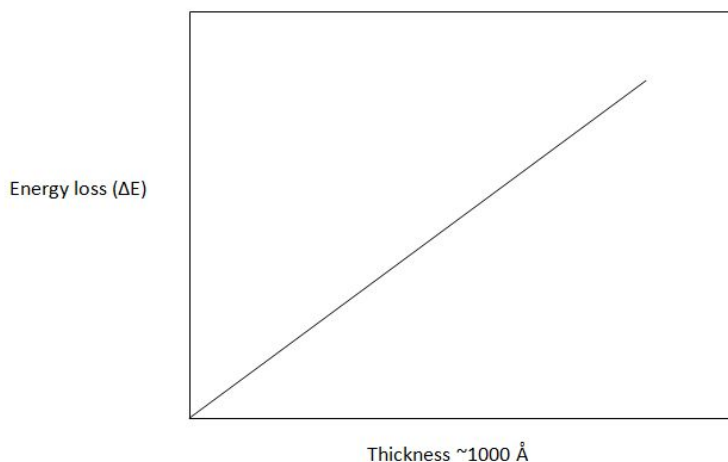


**Figure 7.3:** Variation of energy loss with the depth of the target in constant  $dE/dx$  approximation.

---

### 7.1.3 Experimental set-up

The apparatus for Rutherford backscattering analysis of thin solid surface typically consist of three components:

1. A source of helium ions.
2. An accelerator to energize the helium ions.
3. A detector to measure the energy of scattered ions.

There are two types of accelerator/ion source available. In single stage accelerator, the  $\text{He}^+$  source is placed within an insulating gas-filled tank (Figure 7.4). It is difficult to install new ion source when it is exhausted in this type of accelerator. Moreover, it is also difficult to achieve particles with energy much more than 1 MeV since it is difficult to apply high voltages in this type of system.

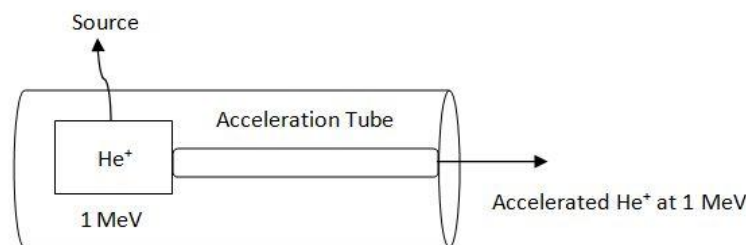


**Figure 7.4:** Schematic representation of a single stage accelerator.

---

Another variation is “tandem accelerator.” Here the ion source is at ground and produces negative ion. The positive terminal is located at the center of the acceleration tube (Figure 7.5). Initially the negative ion is accelerated from ground to terminal. At terminal two-electron stripping process converts the  $\text{He}^-$  to  $\text{He}^{++}$ . The positive ions are further accelerated toward ground due to columbic repulsion from positive terminal. This arrangement can achieve highly accelerated  $\text{He}^{++}$  ions ( $\sim 2.25$  MeV) with moderate voltage of 750 kV.

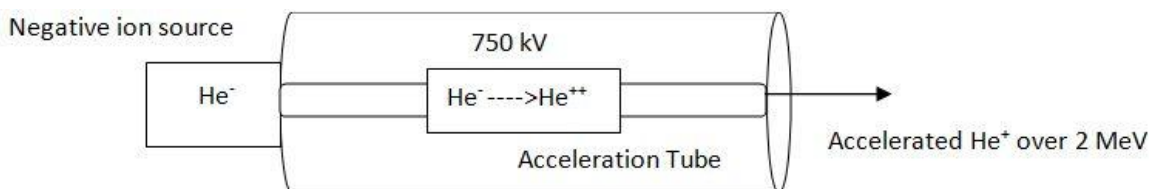


**Figure 7.5:** Schematic representation of a tandem accelerator.

---

Particles that are backscattered by surface atoms of the bombarded specimen are detected by a surface barrier detector. The surface barrier detector is a thin layer of p-type silicon on the n-type substrate resulting p-n junction. When the scattered ions exchange energy with the electrons on the surface of the detector upon reaching the detector, electrons get promoted from the valence band to the conduction band. Thus, each exchange of energy creates electron-hole pairs. The energy of scattered ions is detected by simply counting the number of electron-hole pairs. The energy resolution of the surface barrier detector in a standard RBS experiment is 12 - 20 keV. The surface barrier detector is generally set between  $90^\circ$  and  $170^\circ$  to the incident beam. Films are usually set normal to the incident beam. A simple layout is shown in Figure 7.6.

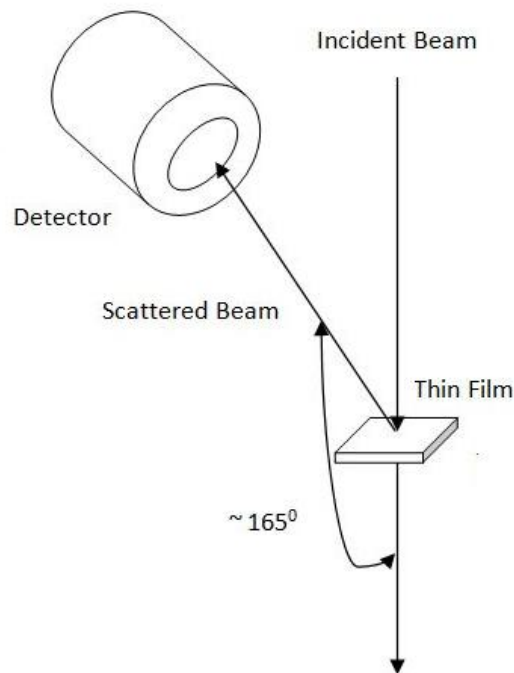


**Figure 7.6:** Schematic representation general set up where the surface barrier detector is placed at angle of  $165^\circ$  to the extrapolated incident beam.

#### 7.1.4 Depth profile analysis

As stated earlier, it is a good approximation in thin film analysis that the total energy loss  $\Delta E$  is proportional to depth  $t$ . With this approximation, we can derive the relation between energy width  $\Delta E$  of the signal from a film of thickness  $\Delta t$  as follows,

$$\Delta E = \Delta t (k \frac{dE}{dx}_{in} + \frac{1}{\cos \emptyset} \frac{dE}{dx}_{out})$$

where  $\emptyset$  = lab scattering angle.

It is worth noting that  $k$  is the kinematic factor defined in equation above and the subscripts “in” and “out” indicate the energies at which the rate of loss of energy or  $dE/dx$  is evaluated. As an example, we consider the backscattering spectrum, at scattering angle  $170^\circ$ , for 2 MeV  $\text{He}^{++}$  incidents on silicon layer deposited onto 2 mm thick niobium substrate Figure 7.7.

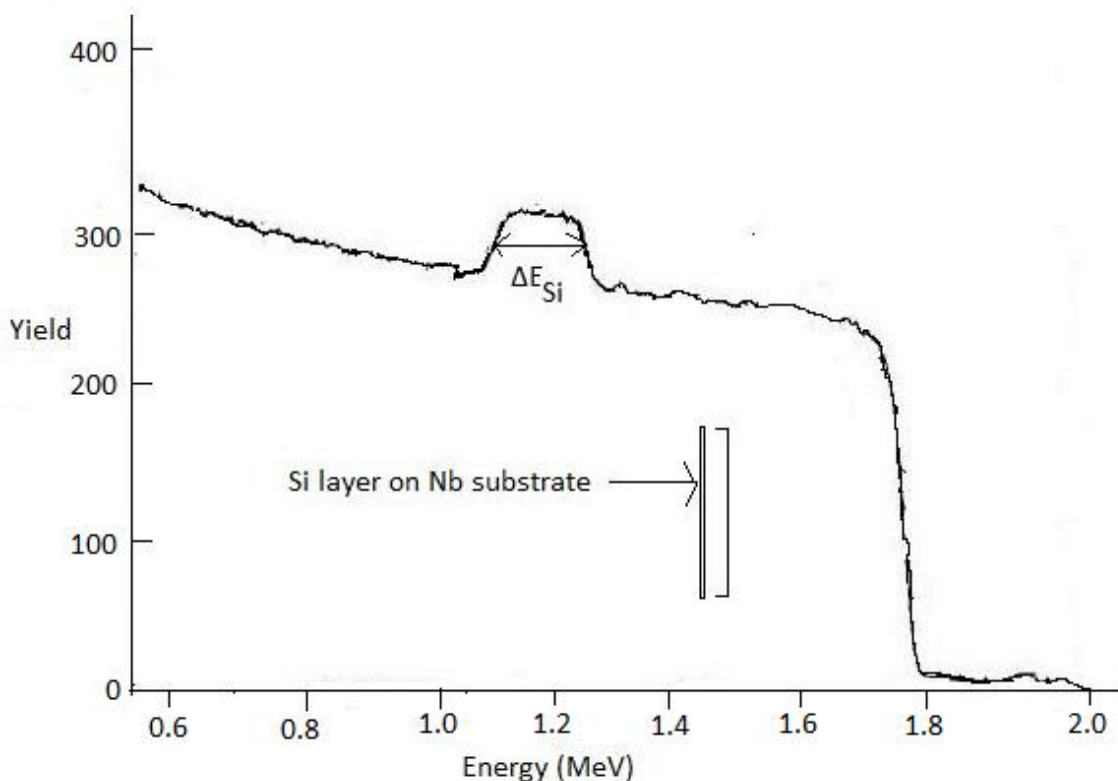


**Figure 7.7:** The backscattering spectrum for 2.0 MeV He ions incident on a silicon thin film deposited onto a niobium substrate. Adapted from P. D. Stupik, M. M. Donovan, A. R. Barron, T. R. Jervis and M. Nastasi, *Thin Solid Films*, 1992, **207**, 138.

The energy loss rate of incoming  $\text{He}^{++}$  or  $dE/dx$  along inward path in elemental Si is  $\approx 24.6 \text{ eV}/\text{\AA}$  at 2 MeV and is  $\approx 26 \text{ eV}/\text{\AA}$  for the outgoing particle at 1.12 MeV (Since  $K$  of Si is 0.56 when the scattering angle is  $170^\circ$ , energy of the outgoing particle would be equal to  $2 \times 0.56$  or 1.12 MeV). Again the value of  $\Delta E_{\text{Si}}$  is  $\approx 133.3 \text{ keV}$ . Putting the values into above equation we get

$$\begin{aligned} \Delta t &\approx 133.3 \text{ keV} / (0.56 * 24.6 \text{ eV}/\text{\AA} + 1/\cos 170^\circ * 26 \text{ eV}/\text{\AA}) \\ &= 133.3 \text{ keV} / (13.77 \text{ eV}/\text{\AA} + 29/.985 \text{ eV}/\text{\AA}) \\ &= 133.3 \text{ keV} / 40.17 \text{ eV}/\text{\AA} \\ &= 3318 \text{ \AA}. \end{aligned}$$

Hence a Si layer of ca. 3300  $\text{\AA}$  thickness has been deposited on the niobium substrate. However we need to remember that the value of  $dE/dx$  is approximated in this calculation.

### 7.1.5 Quantitative Analysis

In addition to depth profile analysis, we can study the composition of an element quantitatively by backscattering spectroscopy. The basic equation for quantitative analysis is

$$Y = \sigma \cdot \Omega \cdot Q \cdot N \Delta t$$

Where  $Y$  is the yield of scattered ions from a thin layer of thickness  $\Delta t$ ,  $Q$  is the number of incident ions and  $\Omega$  is the detector solid angle, and  $N\Delta t$  is the number of specimen atoms ( $\text{atom}/\text{cm}^2$ ). shows the RBS spectrum for a sample of silicon deposited on a niobium substrate and subjected to laser mixing. The Nb has reacted with the silicon to form a  $\text{NbSi}_2$  interphase layer. The Nb signal has broadened after the reaction as show in .

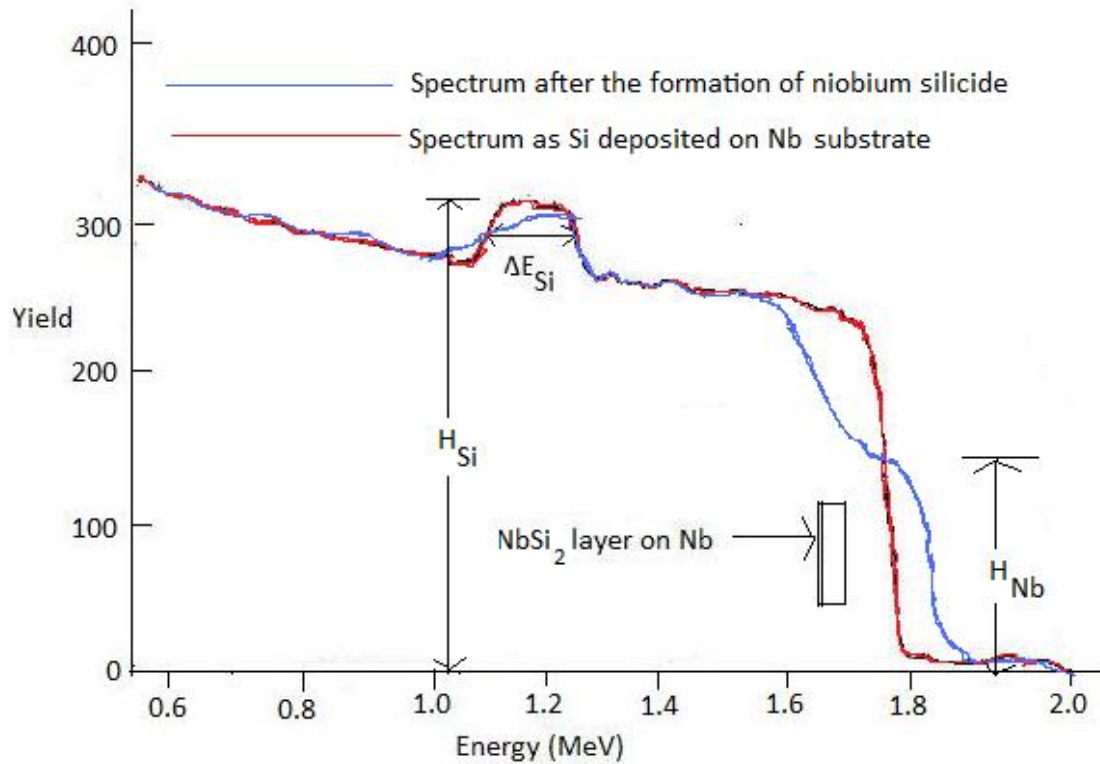


**Figure 7.8:** Backscattering spectra of Si diffused into Nb and Si as deposited on Nb substrate. Adapted from P. D. Stupik, M. M. Donovan, A. R. Barron, T. R. Jervis and M. Nastasi, *Thin Solid Films*, 1992, 207, 138.

We can use ratio of the heights  $H_{\text{Si}}/H_{\text{Nb}}$  of the backscattering spectrum after formation of  $\text{NbSi}_2$  to determine the composition of the silicide layer. The stoichiometric ratio of Nb and Si can be approximated as,

$$N_{\text{Si}}/N_{\text{Nb}} \approx [H_{\text{Si}} * \sigma_{\text{Si}}]/[H_{\text{Nb}} * \sigma_{\text{Nb}}]$$

Hence the concentration of Si and Nb can be determined if we can know the appropriate cross sections  $\sigma_{\text{Si}}$  and  $\sigma_{\text{Nb}}$ . However the yield in the backscattering spectra is better represented as the product of signal height and the energy width  $\Delta E$ . Thus stoichiometric ratio can be better approximated as

$$N_{\text{Si}}/N_{\text{Nb}} \approx [H_{\text{Si}} * \Delta E_{\text{Si}} * \sigma_{\text{Si}}]/[H_{\text{Nb}} * \Delta E_{\text{Nb}} * \sigma_{\text{Nb}}]$$

### 7.1.6 Limitations

It is of interest to understand the limitations of the backscattering technique in terms of the comparison with other thin film analysis technique such as AES, XPS and SIMS (Table 7.1). AES has better mass resolution, lateral resolution and depth resolution than RBS. But AES suffers from sputtering artifacts. Compared to RBS, SIMS has better sensitivity. RBS does not provide any chemical bonding information which we can get from XPS. Again, sputtering artifact problems are also associated in XPS. The strength of RBS lies in quantitative analysis. However, conventional RBS systems cannot analyze ultrathin films since the depth resolution is only about 10 nm using surface barrier detector.

### 7.1.7 Summary

Rutherford Backscattering analysis is a straightforward technique to determine the thickness and composition of thin films ( $< 4000 \text{ \AA}$ ). Areas that have been lately explored are the use of backscattering technique in composition determination of new superconductor oxides; analysis of lattice mismatched epitaxial layers, and as a probe of thin film morphology and surface clustering.

### 7.1.8 Bibliography

- L. C. Feldman and J. W. Mayer, *Fundamentals of Surface and Thin Film Analysis*, North Holland-Elsevier, New York (1986).
- *Ion Spectroscopies for Surface Analysis*, Ed. A. W. Czanderna and D. M. Hercules, Plenum Press (New York), 1991.
- P. D. Stupik, M. M. Donovan, A. R. Barron, T. R. Jervis, and M. Nastasi, *Thin Solid Films*, 1992, **207**, 138

## 7.2 The Application of VSI (Vertical Scanning Interferometry) to the Study of Crystal Surface Processes<sup>2</sup>

### 7.2.1 Introduction

The processes which occur at the surfaces of crystals depend on many external and internal factors such as crystal structure and composition, conditions of a medium where the crystal surface exists and others. The appearance of a crystal surface is the result of complexity of interactions between the crystal surface and the environment. The mechanisms of surface processes such as dissolution or growth are studied by the physical chemistry of surfaces. There are a lot of computational techniques which allows us to predict the changing of surface morphology of different minerals which are influenced by different conditions such as temperature, pressure, pH and chemical composition of solution reacting with the surface. For example, Monte Carlo method is widely used to simulate the dissolution or growth of crystals. However, the theoretical models of surface processes need to be verified by natural observations. We can extract a lot of useful information about the surface processes through studying the changing of crystal surface structure under influence of environmental conditions. The changes in surface structure can be studied through the observation of crystal surface topography. The topography can be directly observed macroscopically or by using microscopic techniques. Microscopic observation allows us to study even very small changes and estimate the rate of processes by observing changing the crystal surface topography in time.

Much laboratory worked under the reconstruction of surface changes and interpretation of dissolution and precipitation kinetics of crystals. Invention of AFM made possible to monitor changes of surface structure during dissolution or growth. However, to detect and quantify the results of dissolution processes or growth it is necessary to determine surface area changes over a significantly larger field of view than AFM can

<sup>2</sup>This content is available online at <http://cnx.org/content/m22326/1.4/>.

provide. More recently, vertical scanning interferometry (VSI) has been developed as new tool to distinguish and trace the reactive parts of crystal surfaces. VSI and AFM are complementary techniques and practically well suited to detect surface changes.

VSI technique provides a method for quantification of surface topography at the angstrom to nanometer level. Time-dependent VSI measurements can be used to study the surface-normal retreat across crystal and other solid surfaces during dissolution process. Therefore, VSI can be used to directly and nondirectly measure mineral dissolution rates with high precision. Analogically, VSI can be used to study kinetics of crystal growth.

### 7.2.2 Physical principles of optical interferometry

Optical interferometry allows us to make extremely accurate measurements and has been used as a laboratory technique for almost a hundred years. Thomas Young observed interference of light and measured the wavelength of light in an experiment, performed around 1801. This experiment gave an evidence of Young's arguments for the wave model for light. The discovery of interference gave a basis to development of interferometry techniques widely successfully used as in microscopic investigations, as in astronomic investigations.

The physical principles of optical interferometry exploit the wave properties of light. Light can be thought as electromagnetic wave propagating through space. If we assume that we are dealing with a linearly polarized wave propagating in a vacuum in  $z$  direction, electric field  $E$  can be represented by a sinusoidal function of distance and time.

$$E(x, y, z, t) = a \cos [2\pi (vt - z/\lambda)] \quad (7.1)$$

Where  $a$  is the amplitude of the light wave,  $v$  is the frequency, and  $\lambda$  is its wavelength. The term within the square brackets is called the phase of the wave. Let's rewrite this equation in more compact form,

$$E(x, y, z, t) = a \cos [\omega t - kz] \quad (7.2)$$

where  $\omega = 2\pi v$  is the circular frequency, and  $k = 2\pi/\lambda$  is the propagation constant. Let's also transform this second equation into a complex exponential form,

$$E(x, y, z, t) = \text{Re}\{a \exp(i\varphi) \exp(i\omega t)\} = \text{Re}\{A \exp(i\omega t)\} \quad (7.3)$$

where  $\varphi = 2\pi z/\lambda$  and  $A = \exp(-i\varphi)$  is known as the complex amplitude. If  $n$  is a refractive index of a medium where the light propagates, the light wave traverses a distance  $d$  in such a medium. The equivalent optical path in this case is

$$p = n \cdot d \quad (7.4)$$

When two light waves are superposed, the result intensity at any point depends on whether reinforce or cancel each other (Figure 7.9). This is well known phenomenon of interference. We will assume that two waves are propagating in the same direction and are polarized with their field vectors in the same plane. We will also assume that they have the same frequency. The complex amplitude at any point in the interference pattern is then the sum of the complex amplitudes of the two waves, so that we can write,

$$A = A_1 + A_2 \quad (7.5)$$

where  $A_1 = a_1 \exp(-i\varphi_1)$  and  $A_2 = a_2 \exp(-i\varphi_2)$  are the complex amplitudes of two waves. The resultant intensity is, therefore,

$$I = |A|^2 = I_1 + I_2 + 2(I_1 I_2)^{1/2} \cos \Delta\varphi \quad (7.6)$$

where  $I_1$  and  $I_2$  are the intensities of two waves acting separately, and  $\Delta\varphi = \varphi_1 - \varphi_2$  is the phase difference between them. If the two waves are derived from a common source, the phase difference corresponds to an optical path difference,

$$\Delta p = (\lambda/2\pi) \Delta\varphi \quad (7.7)$$

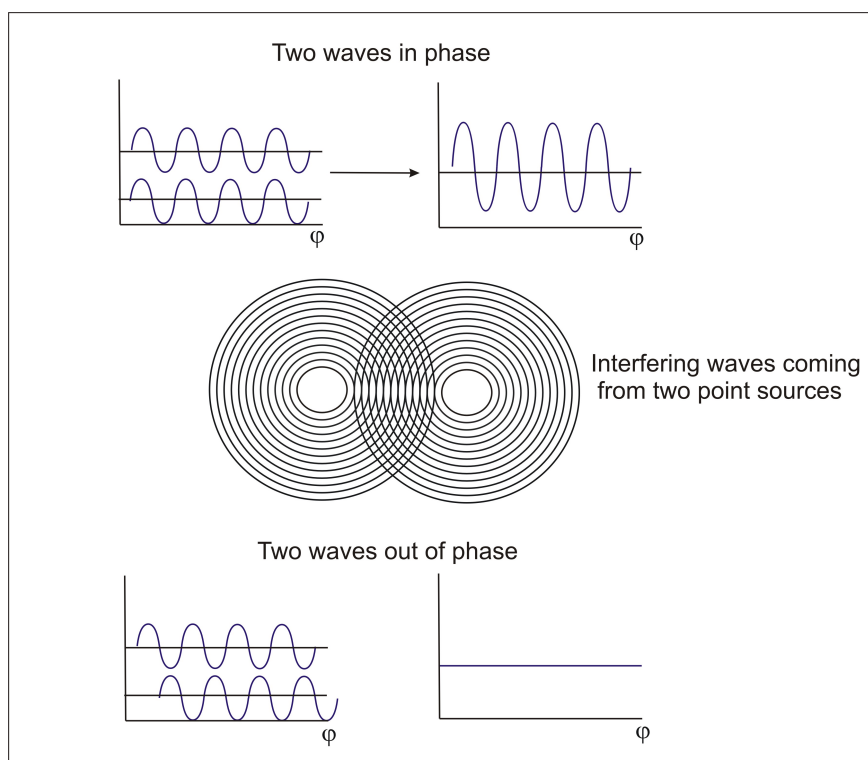


**Figure 7.9:** The scheme of interferometric wave interaction when two waves interact with each other, the amplitude of resulting wave will increase or decrease. The value of this amplitude depends on phase difference between two original waves.

If  $\Delta\varphi$ , the phase difference between the beams, varies linearly across the field of view, the intensity varies sinusoidally, giving rise to alternating light and dark bands or fringes (Figure 7.9). The intensity in an interference pattern has its maximum value

$$I_{\max} = I_1 + I_2 + 2(I_1 I_2)^{1/2} \quad (7.8)$$

when  $\Delta\varphi = 2m\pi$ , where  $m$  is an integer and its minimum value

$$I_{\min} = I_1 + I_2 - 2(I_1 I_2)^{1/2} \quad (7.9)$$

when  $\Delta\varphi = (2m + 1)\pi$ .

The principle of interferometry is widely used to develop many types of interferometric set ups. One of the earliest set ups is Michelson interferometry. The idea of this interferometry is quite simple: interference

fringes are produced by splitting a beam of monochromatic light so that one beam strikes a fixed mirror and the other a movable mirror. An interference pattern results when the reflected beams are brought back together. The Michelson interferometric scheme is shown in Figure 7.10.

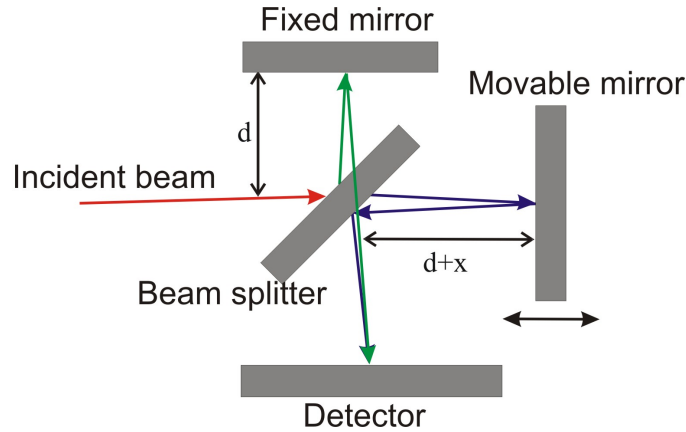


**Figure 7.10:** Schematic representation of a Michelson interferometry set-up.

The difference of path lengths between two beams is  $2x$  because beams traverse the designated distances twice. The interference occurs when the path difference is equal to integer numbers of wavelengths,

$$\Delta p = 2x = m\lambda, m = 0, \pm 1, \pm 2... \quad (7.10)$$

Modern interferometric systems are more complicated. Using special phase-measurement techniques they are capable of performing much more accurate height measurements than can be obtained just by directly looking at the interference fringes and measuring how they depart from being straight and equally spaced. Typically an interferometric system consists of a light source, beamsplitter, objective system, system of registration of signals, and transformation into digital format and computer which processes the data. Vertical scanning interferometry contains all these parts. Figure 7.11 shows a configuration of VSI interferometric system.

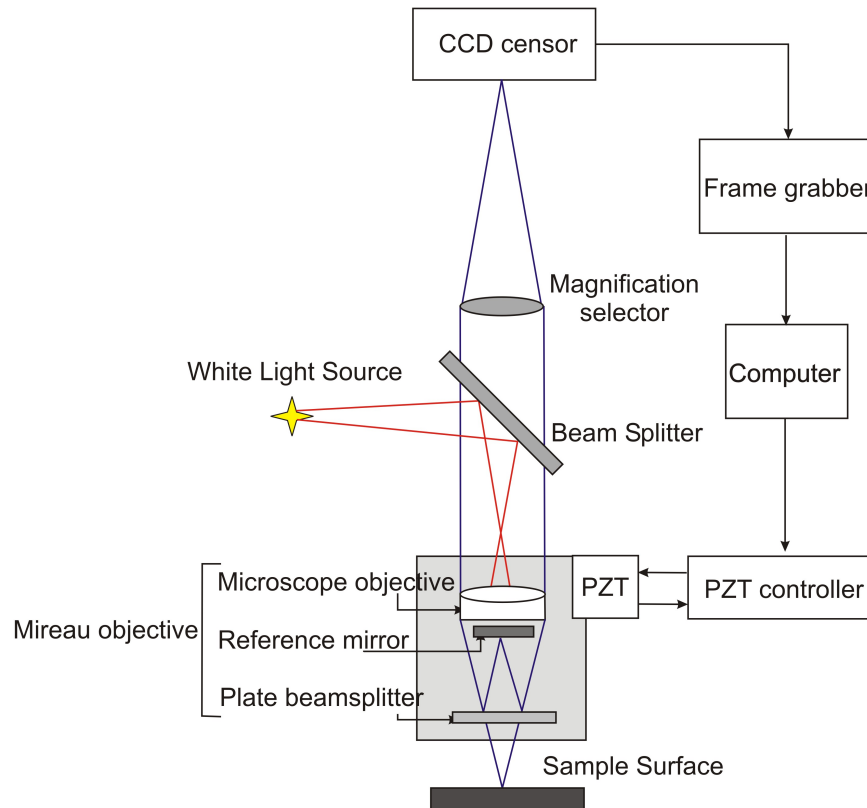


**Figure 7.11:** Schematic representation of the Vertical scanning interferometry (VSI) system.

Many of modern interferometric systems use Mirau objective in their constructions. Mireau objective is based on a Michelson interferometer. This objective consists of a lens, a reference mirror and a beamsplitter. The idea of getting interfering beams is simple: two beams (red lines) travel along the optical axis. Then they are reflected from the reference surface and the sample surface respectively (blue lines). After this these beams are recombined to interfere with each other. An illumination or light source system is used to direct light onto a sample surface through a cube beam splitter and the Mireau objective. The sample surface within the field of view of the objective is uniformly illuminated by those beams with different incidence angles. Any point on the sample surface can reflect those incident beams in the form of divergent cone. Similarly, the point on the reference symmetrical with that on the sample surface also reflects those illuminated beams in the same form.

The Mireau objective directs the beams reflected of the reference and the sample surface onto a CCD (charge-coupled device) sensor through a tube lens. The CCD sensor is an analog shift register that enables the transportation of analog signals (electric charges) through successive stages (capacitors), controlled by a clock signal. The resulting interference fringe pattern is detected by CCD sensor and the corresponding signal is digitized by a frame grabber for further processing with a computer.

The distance between a minimum and a maximum of the interferogram produced by two beams reflected from the reference and sample surface is known. That is, exactly half the wavelength of the light source. Therefore, with a simple interferogram the vertical resolution of the technique would be also limited to  $\lambda/2$ . If we will use a laser light as a light source with a wavelength of 300 nm the resolution would be only 150

nm. This resolution is not good enough for a detailed near-atomic scale investigation of crystal surfaces. Fortunately, the vertical resolution of the technique can be improved significantly by moving either the reference or the sample by a fraction of the wavelength of the light. In this way, several interferograms are produced. Then they are all overlaid, and their phase shifts compared by the computer software Figure 7.12. This method is widely known as phase shift interferometry (PSI).

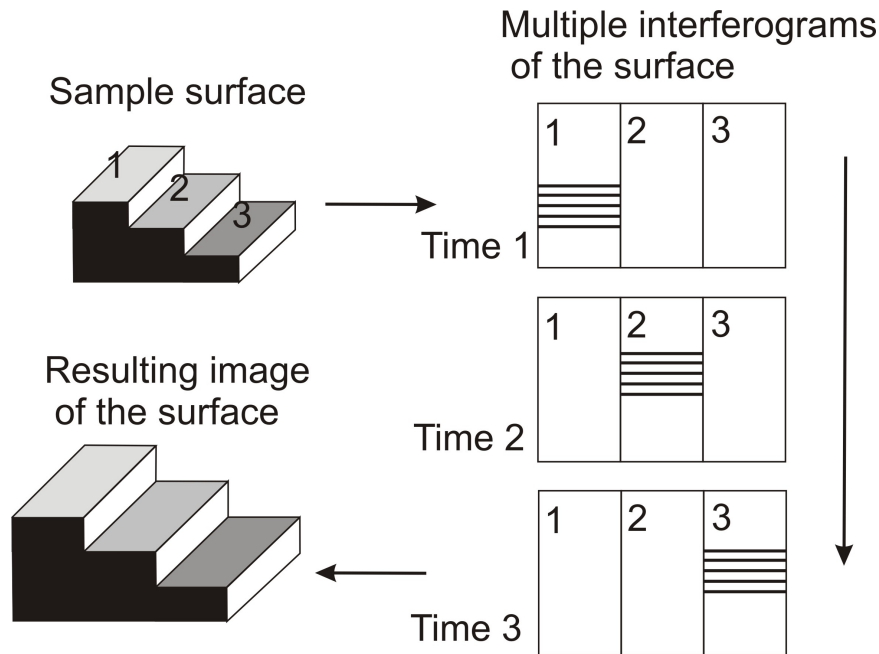


**Figure 7.12:** Sketch illustrating phase-shift technology. The sample is continuously moved along the vertical axes in order to scan surface topography. All interferograms are automatically overlaid using computer software.

Most optical testing interferometers now use phase-shifting techniques not only because of high resolution but also because phase-shifting is a high accuracy rapid way of getting the interferogram information into the computer. Also usage of this technique makes the inherent noise in the data taking process very low. As the result in a good environment angstrom or sub-angstrom surface height measurements can be performed. As it was said above, in phase-shifting interferometry the phase difference between the interfering beams is changed at a constant rate as the detector is read out. Once the phase is determined across the interference field, the corresponding height distribution on the sample surface can be determined. The phase distribution  $\phi(x, y)$  is recorded by using the CCD camera.

Let's assign  $A(x, y)$ ,  $B(x, y)$ ,  $C(x, y)$  and  $D(x, y)$  to the resulting interference light intensities which are corresponded to phase-shifting steps of  $0$ ,  $\pi/2$ ,  $\pi$  and  $3\pi/2$ . These intensities can be obtained by moving the reference mirror through displacements of  $\lambda/8$ ,  $\lambda/4$  and  $3\lambda/8$ , respectively. The equations for the resulting intensities would be:

$$A(x, y) = I_1(x, y) + I_2(x, y) \cos \alpha(x, y) \quad (7.11)$$

$$B(x, y) = I_1(x, y) - I_2(x, y) \sin \alpha(x, y) \quad (7.12)$$

$$C(x, y) = I_1(x, y) - I_2(x, y) \cos\alpha(x, y) \quad (7.13)$$

$$D(x, y) = I_1(x, y) + I_2(x, y) \sin\alpha(x, y) \quad (7.14)$$

where  $I_1(x, y)$  and  $I_2(x, y)$  are two overlapping beams from two symmetric points on the test surface and the reference respectively. Solving equations (7.11)–(7.14), the phase map  $\phi(x, y)$  of a sample surface will be given by the relation:

$$\varphi(x, y) = \frac{B(x, y) - D(x, y)}{A(x, y) - C(x, y)} \quad (7.15)$$

Once the phase is determined across the interference field pixel by pixel on a two-dimensional CCD array, the local height distribution/contour,  $h(x, y)$ , on the test surface is given by

$$h(x, y) = \frac{\lambda}{4\pi} \varphi(x, y) \quad (7.16)$$

Normally the resulted fringe can be in the form of a linear fringe pattern by adjusting the relative position between the reference mirror and sample surfaces. Hence any distorted interference fringe would indicate a local profile/contour of the test surface.

It is important to note that the Mireau objective is mounted on a capacitive closed-loop controlled PZT (piezoelectric actuator) as to enable phase shifting to be accurately implemented. The PZT is based on piezoelectric effect referred to the electric potential generated by applying pressure to piezoelectric material. This type of materials is used to convert electrical energy to mechanical energy and vice-versa. The precise motion that results when an electric potential is applied to a piezoelectric material has an importance for nanopositioning. Actuators using the piezo effect have been commercially available for 35 years and in that time have transformed the world of precision positioning and motion control.

Vertical scanning interferometer also has another name; white-light interferometry (WLI) because of using the white light as a source of light. With this type of source a separate fringe system is produced for each wavelength, and the resultant intensity at any point of examined surface is obtained by summing these individual patterns. Due to the broad bandwidth of the source the coherent length  $L$  of the source is short:

$$L = \frac{\lambda^2}{n\Delta\lambda} \quad (7.17)$$

where  $\lambda$  is the center wavelength,  $n$  is the refractive index of the medium,  $\Delta\lambda$  is the spectral width of the source. In this way good contrast fringes can be obtained only when the lengths of interfering beams pathways are closed to each other. If we will vary the length of a pathway of a beam reflected from sample, the height of a sample can be determined by looking at the position for which a fringe contrast is a maximum. In this case interference pattern exist only over a very shallow depth of the surface. When we vary a pathway of sample-reflected beam we also move the sample in a vertical direction in order to get the phase at which maximum intensity of fringes will be achieved. This phase will be converted in height of a point at the sample surface.

The combination of phase shift technology with white-light source provides a very powerful tool to measure the topography of quite rough surfaces with the amplitude in heights about and the precision up to 1-2 nm. Through a developed software package for quantitatively evaluating the resulting interferogram, the proposed system can retrieve the surface profile and topography of the sample objects Figure 7.13.

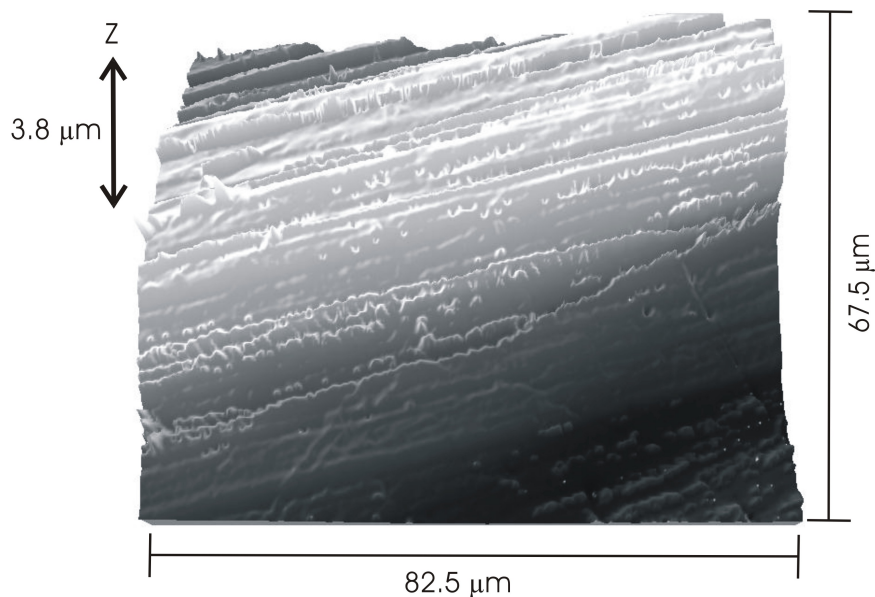


**Figure 7.13:** Example of muscovite surface topography, obtained by using VSI- 50x objective.

---

### 7.2.3 A comparison of common methods to determine surface topography: SEM, AFM and VSI

Except the interferometric methods described above, there are a several other microscopic techniques for studying crystal surface topography. The most common are scanning electron microscopy (SEM) and atomic force microscopy (AFM). All these techniques are used to obtain information about the surface structure. However they differ from each other by the physical principles on which they based.

#### 7.2.3.1 Scanning electron microscopy

SEM allows us to obtain images of surface topography with the resolution much higher than the conventional light microscopes do. Also it is able to provide information about other surface characteristics such as chemical composition, electrical conductivity etc, see Figure 7.14. All types of data are generated by the reflecting of accelerated electron beams from the sample surface. When electrons strike the sample surface, they lose their energy by repeated random scattering and adsorption within an outer layer into the depth varying from 100 nm to 5 microns.

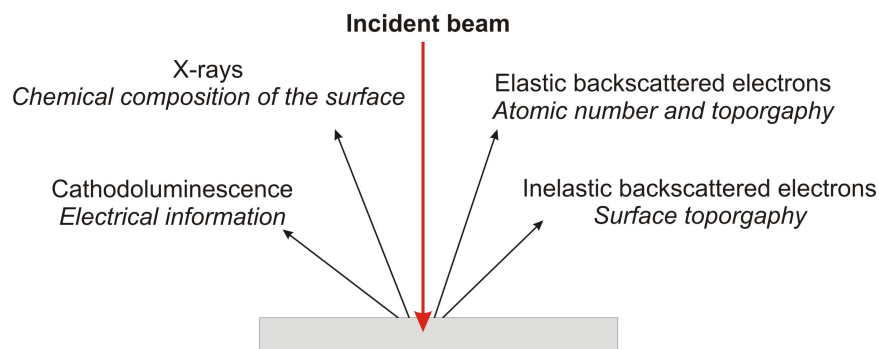


**Figure 7.14:** Scheme of electron beam-sample interaction at SEM analysis

The thickness of this outer layer also known as interactive layer depends on energy of electrons in the beam, composition and density of a sample. Result of the interaction between electron beam and the surface provides several types of signals. The main type is secondary or inelastic scattered electrons. They are produced as a result of interaction between the beam of electrons and weakly bound electrons in the conduction band of the sample. Secondary electrons are ejected from the  $k$ -orbitals of atoms within the surface layer of thickness about a few nanometers. This is because secondary electrons are low energy electrons ( $<50$  eV), so only those formed within the first few nanometers of the sample surface have enough energy to escape and be detected. Secondary backscattered electrons provide the most common signal to investigate surface topography with lateral resolution up to 0.4 - 0.7 nm.

High energy beam electrons are elastic scattered back from the surface. This type of signal gives information about chemical composition of the surface because the energy of backscattered electrons depends on the weight of atoms within the interaction layer. Also this type of electrons can form secondary electrons and escape from the surface or travel farther into the sample than the secondary. The SEM image formed is the result of the intensity of the secondary electron emission from the sample at each  $x,y$  data point during the scanning of the surface.

### 7.2.3.2 Atomic force microscopy

AFM is a very popular tool to study surface dissolution. AFM set up consists of scanning a sharp tip on the end of a flexible cantilever which moves across a sample surface. The tips typically have an end radius of 2 to 20 nm, depending on tip type. When the tip touches the surface the forces of these interactions lead to deflection of a cantilever. The interaction between tip and sample surface involves mechanical contact forces, van der Waals forces, capillary forces, chemical bonding, electrostatic forces, magnetic forces etc. The deflection of a cantilever is usually measured by reflecting a laser beam off the back of the cantilever into a split photodiode detector. A schematic drawing of AFM can be seen in Figure 7.15. The two most commonly used modes of operation are contact mode AFM and tapping mode AFM, which are conducted in air or liquid environments.

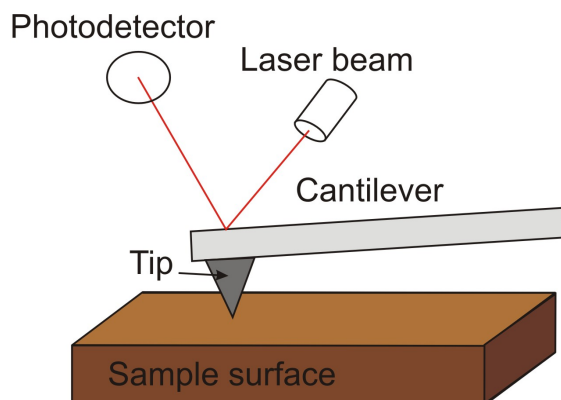


**Figure 7.15:** Schematic drawing of an AFM apparatus.

Working under the contact mode AFM scans the sample while monitoring the change in cantilever deflection with the split photodiode detector. Loop maintains a constant cantilever reflection by vertically moving the scanner to get a constant signal. The distance which the scanner goes by moving vertically at each x,y data point is stored by the computer to form the topographic image of the sample surface. Working under the tapping mode AFM oscillates the cantilever at its resonance frequency (typically  $\sim 300$  kHz) and lightly “taps” the tip on the surface during scanning. The electrostatic forces increase when tip gets close to the sample surface, therefore the amplitude of the oscillation decreases. The laser deflection method is used to detect the amplitude of cantilever oscillation. Similar to the contact mode, feedback loop maintains a constant oscillation amplitude by moving the scanner vertically at every x,y data point. Recording this movement forms the topographical image. The advantage of tapping mode over contact mode is that it eliminates the lateral, shear forces present in contact mode. This enables tapping mode to image soft, fragile, and adhesive surfaces without damaging them while work under contact mode allows the damage to occur.

### 7.2.3.3 Comparison of techniques

All techniques described above are widely used in studying of surface nano- and micromorphology. However, each method has its own limitations and the proper choice of analytical technique depends on features of analyzed surface and primary goals of research.

All these techniques are capable to obtain an image of a sample surface with quite good resolution. The lateral resolution of VSI is much less, then for other techniques: 150 nm for VSI and 0.5 nm for AFM and SEM. Vertical resolution of AFM (0.5 Å) is better then for VSI (1 - 2 nm), however VSI is capable to measure a high vertical range of heights (1 mm) which makes possible to study even very rough surfaces. On the contrary, AFM allows us to measure only quite smooth surfaces because of its relatively small vertical scan range (7  $\mu\text{m}$ ). SEM has less resolution, than AFM because it requires coating of a conductive material with the thickness within several nm.

The significant advantage of VSI is that it can provide a large field of view (845  $\times$  630  $\mu\text{m}$  for 10x objective) of tested surfaces. Recent studies of surface roughness characteristics showed that the surface roughness parameters increase with the increasing field of view until a critical size of 250,000  $\mu\text{m}$  is reached. This value is larger then the maximum field of view produced by AFM (100  $\times$  100  $\mu\text{m}$ ) but can be easily obtained by VSI. SEM is also capable to produce images with large field of view. However, SEM is able to provide only 2D images from one scan while AFM and VSI let us to obtain 3D images. It makes quantitative

analysis of surface topography more complicated, for example, topography of membranes is studied by cross section and top view images.

	VSI	AFM	SEM
Lateral resolution	0.5-1.2 $\mu\text{m}$	0.5 nm	0.5-1 nm
Vertical resolution	2 nm	0.5 $\text{\AA}$	Only 2D images
Field of view	845 $\times$ 630 $\mu\text{m}$ (10x objective)	100 $\times$ 100 $\mu\text{m}$	1-2 mm
Vertical range of scan	1 mm	10 $\mu\text{m}$	-
Preparation of a sample	-	-	Required coating of a conducted material
Required environment	Air	Air, liquid	Vacuum

**Table 7.2:** A comparison of VSI sample and resolution with AFM and SEM.

#### 7.2.4 The experimental studying of surface processes using microscopic techniques

The limitations of each technique described above are critically important to choose appropriate technique for studying surface processes. Let's explore application of these techniques to study dissolution of crystals.

When crystalline matter dissolves the changes of the crystal surface topography can be observed by using microscopic techniques. If we will apply an unreactive mask (silicon for example) on crystal surface and place a crystalline sample into the experiment reactor then we get two types of surfaces: dissolving and remaining the same or unreacted. After some period of time the crystal surface starts to dissolve and change its z-level. In order to study these changes *ex situ* we can pull out a sample from the reaction cell then remove a mask and measure the average height difference  $\Delta \bar{h}$  between the unreacted and dissolved areas. The average heights of dissolved and unreacted areas are obtained through digital processing of data obtained by microscopes. The velocity of normal surface retreat  $v_{\text{SNR}}$  during the time interval  $\Delta t$  is defined as

$$v_{\text{SNR}} = \frac{\Delta \bar{h}}{\Delta t}$$

Dividing this velocity by the molar volume  $\bar{V}$  ( $\text{cm}^3/\text{mol}$ ) gives a global dissolution rate in the familiar units of moles per unit area per unit time:

$$R = \frac{v_{\text{SNR}}}{\bar{V}} \quad (7.18)$$

This method allows us to obtain experimental values of dissolution rates just by precise measuring of average surface heights. Moreover, using this method we can measure local dissolution rates at etch pits by monitoring changes in the volume and density of etch pits across the surface over time. VSI technique is capable to perform these measurements because of large vertical range of scanning. In order to get precise values of rates which are not depend on observing place of crystal surface we need to measure enough large areas. VSI technique provides data from areas which are large enough to study surfaces with heterogeneous dissolution dynamics and obtain average dissolution rates. Therefore, VSI makes possible to measure rates of normal surface retreat during the dissolution and observe formation, growth and distribution of etch pits on the surface.

However, if the mechanism of dissolution is controlled by dynamics of atomic steps and kink sites within a smooth atomic surface area, the observation of the dissolution process need to use a more precise technique. AFM is capable to provide information about changes in step morphology *in situ* when the dissolution

occurs. For example, immediate response of the dissolved surface to the changing of environmental conditions (concentrations of ions in the solution, pH etc.) can be studied by using AFM.

SEM is also used to examine micro and nanotexture of solid surfaces and study dissolution processes. This method allows us to observe large areas of crystal surface with high resolution which makes possible to measure a high variety of surfaces. The significant disadvantage of this method is the requirement to cover examine sample by conductive substance which limits the resolution of SEM. The other disadvantage of SEM is that the analysis is conducted in vacuum. Recent technique, environmental SEM or ESEM overcomes these requirements and makes possible even examine liquids and biological materials. The third disadvantage of this technique is that it produces only 2D images. This creates some difficulties to measure  $\Delta\bar{h}$  within the dissolving area. One of advantages of this technique is that it is able to measure not only surface topography but also chemical composition and other surface characteristics of the surface. This fact is used to monitor changing in chemical composition during the dissolution.

### 7.2.5 Bibliography

- A. C. Lasaga, *Kinetic Theory in the Earth Sciences*. Princeton Univ. Press, Princeton, NJ (1998).
- A. Luttge, E. V. Bolton, and A. C. Lasaga A.C., *Am. J. Sci.*, 1999, **299**, 652.
- D. Kaczmarek, *Vacuum*, 2001, **62**, 303.
- P. Hariharan. *Optical interferometry*, Second edition, Academic press (2003) ISBN 0-12-311630-9.
- A. Luttge and P. G. Conrad, *Appl. Environ. Microbiol.*, 2004, **70**, 1627.
- A. C. Lasaga and A. Luttge, *American Mineralogist*, 2004, **89**, 527.
- K. J. Davis and A. Luttge, *Am. J. Sci.*, 2005, **305**, 727.
- S. H. Wang and Tay, *Meas. Sci. Technol.*, 2006, **17**, 617.
- A. Luttge and R. S. Arvidson, in *Kinetics of water-rock interaction*, Ed. S. Brantley, J. Kubicki, and A. White, Springer (2007).
- L. Zhang and A. Luttge, *American Mineralogist*, 2007, **92**, 1316.
- C. Fischer A. and Luttge, *Am. J. Sci.*, 2007, **307**, 955.
- Y. Wyart, G. Georges, C. Deumie, C. Amra, and P. Moulina, *J. Membrane Sci.*, 2008, **315**, 82.
- T. C. Vaimakis, E. D. Economou, and C. C. Trapalis, *J. Therm. Anal. Cal.*, 2008, **92**, 783.

## 7.3 Atomic Force Microscopy<sup>3</sup>

### 7.3.1 Introduction

Atomic force microscopy (AFM) is a high-resolution form of scanning probe microscopy, also known as scanning force microscopy (SFM). The instrument uses a cantilever with a sharp tip at the end to scan over the sample surface (Figure 7.16). As the probe scans over the sample surface, attractive or repulsive forces between the tip and sample, usually in the form of van der Waal forces but also can be a number of others such as electrostatic and hydrophobic/hydrophilic, cause a deflection of the cantilever. The deflection is measured by a laser (Figure 7.16) which is reflected off the cantilever into photodiodes. As one of the photodiodes collects more light, it creates an output signal that is processed and provides information about the vertical bending of the cantilever. This data is then sent to a scanner that controls the height of the probe as it moves across the surface. The variance in height applied by the scanner can then be used to produce a three-dimensional topographical representation of the sample.

<sup>3</sup>This content is available online at <<http://cnx.org/content/m34664/1.1/>>.

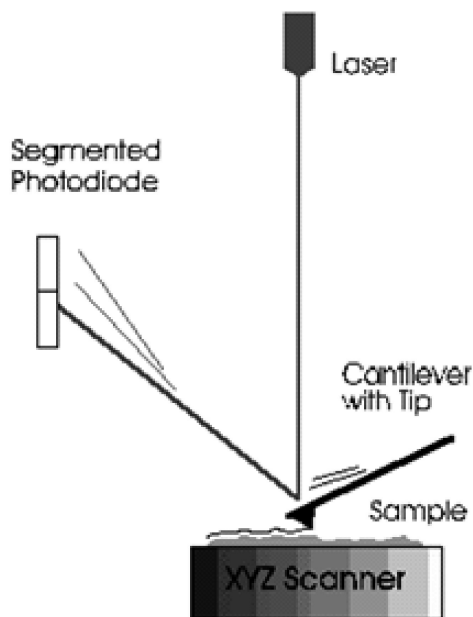


**Figure 7.16:** Simple schematic of atomic force microscope (AFM) apparatus. Adapted from H. G. Hansma, Department of Physics, University of California, Santa Barbara.

---

## 7.3.2 Modes of operation

### 7.3.2.1 Contact mode

The contact mode method utilizes a constant force for tip-sample interactions by maintaining a constant tip deflection (Figure 7.17). The tip communicates the nature of the interactions that the probe is having at the surface via feedback loops and the scanner moves the entire probe in order to maintain the original deflection of the cantilever. The constant force is calculated and maintained by using Hooke's Law, (7.19). This equation relates the force ( $F$ ), spring constant ( $k$ ), and cantilever deflection ( $x$ ). Force constants typically range from 0.01 to 1.0 N/m. Contact mode usually has the fastest scanning times but can deform the sample surface. It is also only the only mode that can attain "atomic resolution."

$$F = -kx \tag{7.19}$$



**Figure 7.17:** Schematic diagram of probe and surface interaction in contact mode.

---

### 7.3.2.2 Tapping mode

In the tapping mode the cantilever is externally oscillated at its fundamental resonance frequency (Figure 7.18). A piezoelectric on top of the cantilever is used to adjust the amplitude of oscillation as the probe scans across the surface. The deviations in the oscillation frequency or amplitude due to interactions between the probe and surface are measured, and provide information about the surface or types of material present in the sample. This method is gentler than contact AFM since the tip is not dragged across the surface, but it does require longer scanning times. It also tends to provide higher lateral resolution than contact AFM.

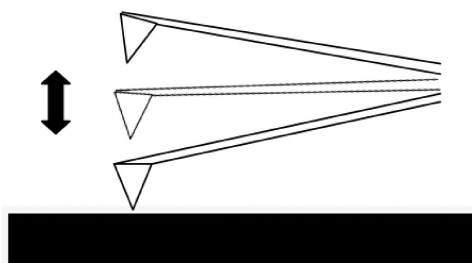


**Figure 7.18:** Diagram of probe and surface interaction in tapping mode.

---

### 7.3.2.3 Noncontact mode

For noncontact mode the cantilever is oscillated just above its resonance frequency and this frequency is decreased as the tip approaches the surface and experiences the forces associated with the material (Figure 7.19). The average tip-to-sample distance is measured as the oscillation frequency or amplitude is kept constant, which then can be used to image the surface. This method exerts very little force on the sample, which extends the lifetime of the tip. However, it usually does not provide very good resolution unless placed under a strong vacuum.

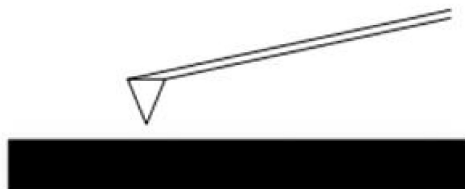


**Figure 7.19:** Diagram of probe and surface interaction in noncontact mode.

---

### 7.3.3 Experimental limitations

A common problem seen in AFM images is the presence of artifacts which are distortions of the actual topography, usually either due to issues with the probe, scanner, or image processing. The AFM scans slowly which makes it more susceptible to external temperature fluctuations leading to thermal drift. This leads to artifacts and inaccurate distances between topographical features.

It is also important to consider that the tip is not perfectly sharp and therefore may not provide the best aspect ratio, which leads to a convolution of the true topography. This leads to features appearing too large or too small since the width of the probe cannot precisely move around the particles and holes on the surface. It is for this reason that tips with smaller radii of curvature provide better resolution in imaging. The tip can also produce false images and poorly contrasted images if it is blunt or broken.

The movement of particles on the surface due to the movement of the cantilever can cause noise, which forms streaks or bands in the image. Artifacts can also be made by the tip being of inadequate proportions compared to the surface being scanned. It is for this reason that it is important to use the ideal probe for the particular application.

### 7.3.4 Sample size and preparation

The sample size varies with the instrument but a typical size is 8 mm by 8 mm with a typical height of 1 mm. Solid samples present a problem for AFM since the tip can shift the material as it scans the surface. Solutions or dispersions are best for applying as uniform of a layer of material as possible in order to get the most accurate value of particles' heights. This is usually done by spin-coating the solution onto freshly cleaved mica which allows the particles to stick to the surface once it has dried.

### 7.3.5 Applications of AFM

AFM is particularly versatile in its applications since it can be used in ambient temperatures and many different environments. It can be used in many different areas to analyze different kinds of samples such as semiconductors, polymers, nanoparticles, biotechnology, and cells amongst others. The most common application of AFM is for morphological studies in order to attain an understanding of the topography of the sample. Since it is common for the material to be in solution, AFM can also give the user an idea of the ability of the material to be dispersed as well as the homogeneity of the particles within that dispersion. It also can provide a lot of information about the particles being studied such as particle size, surface area, electrical properties, and chemical composition. Certain tips are capable of determining the principal mechanical, magnetic, and electrical properties of the material. For example, in magnetic force microscopy (MFM) the probe has a magnetic coating that senses magnetic, electrostatic, and atomic interactions with the surface.

This type of scanning can be performed in static or dynamic mode and depicts the magnetic structure of the surface.

### 7.3.5.1 AFM of carbon nanotubes

Atomic force microscopy is usually used to study the topographical morphology of these materials. By measuring the thickness of the material it is possible to determine if bundling occurred and to what degree. Other dimensions of the sample can also be measured such as the length and width of the tubes or bundles. It is also possible to detect impurities, functional groups (Figure 7.20), or remaining catalyst by studying the images. Various methods of producing nanotubes have been found and each demonstrates a slightly different profile of homogeneity and purity. These impurities can be carbon coated metal, amorphous carbon, or other allotropes of carbon such as fullerenes and graphite. These facts can be utilized to compare the purity and homogeneity of the samples made from different processes, as well as monitor these characteristics as different steps or reactions are performed on the material. The distance between the tip and the surface has proven itself to be an important parameter in noncontact mode AFM and has shown that if the tip is moved past the threshold distance, approximately  $30\ \mu\text{m}$ , it can move or damage the nanotubes. If this occurs, a useful characterization cannot be performed due to these distortions of the image.

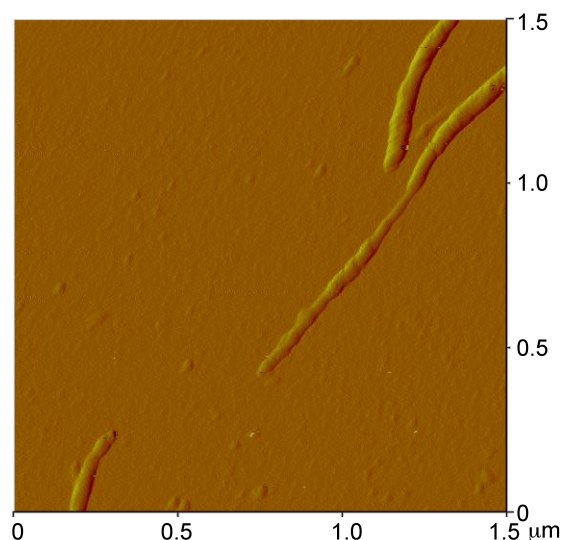


**Figure 7.20:** AFM image of a polyethyleneimine-functionalized single walled carbon nanotube (PEI-SWNT) showing the presence of PEI “globules” on the SWNT. Adapted from E. P. Dillon, C. A. Crouse, and A. R. Barron, *ACS Nano*, 2008, **2**, 156.

---

### 7.3.5.2 AFM of fullerenes

Atomic force microscopy is best applied to aggregates of fullerenes rather than individual ones. While the AFM can accurately perform height analysis of individual fullerene molecules, it has poor lateral resolution and it is difficult to accurately depict the width of an individual molecule. Another common issue that arises with contact AFM and fullerene deposited films is that the tip shifts clusters of fullerenes which can lead to discontinuities in sample images.

### 7.3.6 Bibliography

- R. Anderson and A. R. Barron, *J. Am. Chem. Soc.*, 2005, **127**, 10458.
- M. Bellucci, G. Gaggiotti, M. Marchetti, F. Micciulla, R. Mucciato, and M. Regi, *J. Physics: Conference Series*, 2007, **61**, 99.
- I. I. Bobrinetskii, V. N. Kukin, V. K. Nevolin, and M. M. Simunin. *Semiconductor*, 2008, **42**, 1496.
- S. H. Cohen and M. L. Lightbody. *Atomic Force Microscopy/Scanning Tunneling Microscopy 2*. Plenum, New York (1997).
- E. P. Dillon, C. A. Crouse, and A. R. Barron, *ACS Nano*, 2008, **2**, 156.
- C. Gu, C. Ray, S. Guo, and B. B. Akhremitchev, *J. Phys. Chem.*, 2007, **111**, 12898.
- G. Kaupp, *Atomic Force Microscopy, Scanning Nearfield Optical Microscopy and Nanoscratching: Application to Rough and Natural Surfaces*. Springer-Verlag, Berlin (2006).
- S. Morita, R. Wiesendanger, E. Meyer, and F. J. Giessibl. *Noncontact Atomic Force Microscopy*. Springer, Berlin (2002).



# Chapter 7

## Materials Characterization

### 7.1 Rutherford Backscattering of Thin Films<sup>1</sup>

#### 7.1.1 Introduction

One of the main research interests of the semiconductor industry is to improve the performance of semi-conducting devices and to construct new materials with reduced size or thickness that have potential application in transistors and microelectronic devices. However, the most significant challenge regarding thin film semiconductor materials is measurement. Properties such as the thickness, composition at the surface, and contamination, all are critical parameters of the thin films. To address these issues, we need an analytical technique which can measure accurately through the depth of the of the semiconductor surface without destruction of the material. Rutherford backscattering spectroscopy is a unique analysis method for this purpose. It can give us information regarding in-depth profiling in a non-destructive manner. However X-ray photo electron spectroscopy (XPS), energy dispersive X-ray analysis (EDX) and Auger electron spectroscopy are also able to study the depth-profile of semiconductor films. Table 7.1 demonstrates the comparison between those techniques with RBS.

Method	Destructive	Incident particle	Outgoing Particle	Detection limit	Depth resolution
RBS	No	Ion	Ion	~1	10 nm
XPS	Yes	X-ray photon	Electron	~0.1-1	~1 $\mu\text{m}$
EDX	Yes	Electron	X-ray photon	~0.1	1.5 nm
Auger	Yes	Electron	Electron	~0.1-1	1.5 nm

**Table 7.1:** Comparison between different thin film analysis techniques.

#### 7.1.2 Basic concept of Rutherford backscattering spectroscopy

At a basic level, RBS demonstrates the electrostatic repulsion between high energy incident ions and target nuclei. The specimen under study is bombarded with monoenergetic beam of  $^4\text{He}^+$  particles and the backscattered particles are detected by the detector-analysis system which measures the energies of the particles. During the collision, energy is transferred from the incident particle to the target specimen atoms; the change in energy of the scattered particle depends on the masses of incoming and target atoms. For an

<sup>1</sup>This content is available online at <<http://cnx.org/content/m22411/1.3/>>.

incident particle of mass  $M_1$ , the energy is  $E_0$  while the mass of the target atom is  $M_2$ . After the collision, the residual energy  $E$  of the particle scattered at angle  $\emptyset$  can be expressed as:

$$E = k^2 E_0$$

$$k = \frac{\left( M_1 \cos \emptyset + \sqrt{M_2^2 - M_1^2 \sin^2 \emptyset} \right)}{M_1 + M_2}$$

where  $k$  is the kinematic scattering factor, which is actually the energy ratio of the particle before and after the collision. Since  $k$  depends on the masses of the incident particle and target atom and the scattering angle, the energy of the scattered particle is also determined by these three parameters. A simplified layout of backscattering experiment is shown in Figure 1 (Figure 7.1).

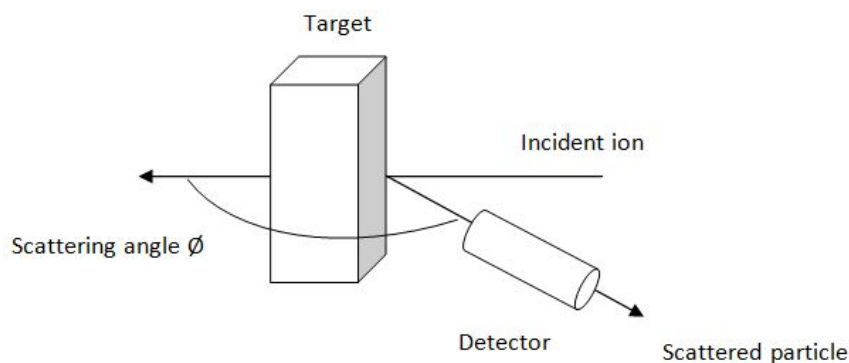


Figure 7.1: Schematic representation of the experimental setup for Rutherford backscattering analysis.

The probability of a scattering event can be described by the differential scattering cross section of a target atom for scattering an incoming particle through the angle  $\emptyset$  into differential solid angle as follows,

$$\frac{d\sigma_R}{d\phi} = \left( \frac{zZe^2}{2E_0 \sin^2 \emptyset} \right) \frac{\left[ \cos \emptyset + \sqrt{1 - \left( \frac{M_1}{M_2} \sin \emptyset \right)^2} \right]^2}{\sqrt{1 - \left( \frac{M_1}{M_2} \sin \emptyset \right)^2}}$$

where  $d\sigma_R$  is the effective differential cross section for the scattering of a particle. The above equation may look complicated but it conveys the message that the probability of scattering event can be expressed as a function of scattering cross section which is proportional to the  $zZ$  when a particle with charge  $ze$  approaches the target atom with charge  $Ze$ .

Helium ions not scattered at the surface lose energy as they traverse the solid. They lose energy due to interaction with electrons in the target. After collision the He particles lose further energy on their way out to the detector. We need to know two quantities to measure the energy loss, the distance  $\Delta t$  that the particles penetrate into the target and the energy loss  $\Delta E$  in this distance Figure 7.2. The rate of energy loss

or stopping power is a critical component in backscattering experiments as it determines the depth profile in a given experiment.

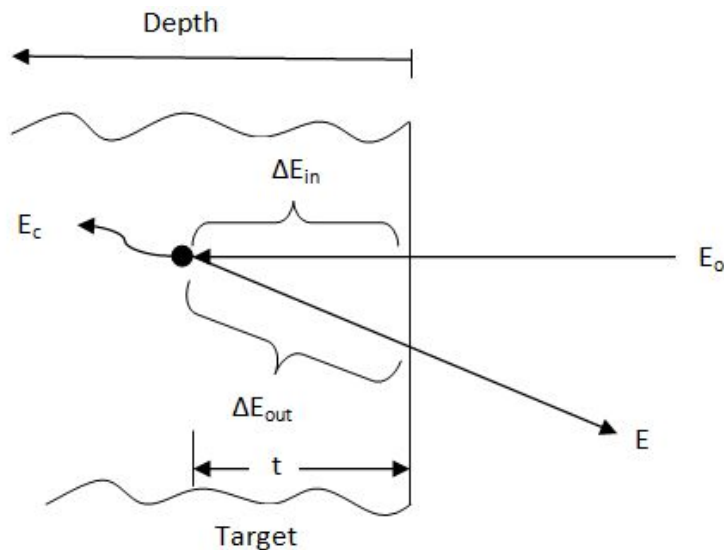


**Figure 7.2:** Components of energy loss for a ion beam that scatters from depth  $t$ . First, incident beam loses energy through interaction with electrons  $\Delta E_{in}$ . Then energy lost occurs due to scattering  $E_c$ . Finally outgoing beam loses energy for interaction with electrons  $\Delta E_{out}$ . Adapted from L. C. Feldman and J. W. Mayer, *Fundamentals of Surface and Thin Film Analysis*, North Holland-Elsevier, New York (1986).

In thin film analysis, it is convenient to assume that total energy loss  $\Delta E$  into depth  $t$  is only proportional to  $t$  for a given target. This assumption allows a simple derivation of energy loss in backscattering as more complete analysis requires many numerical techniques. In constant  $dE/dx$  approximation, total energy loss becomes linearly related to depth  $t$ , Figure 7.3.

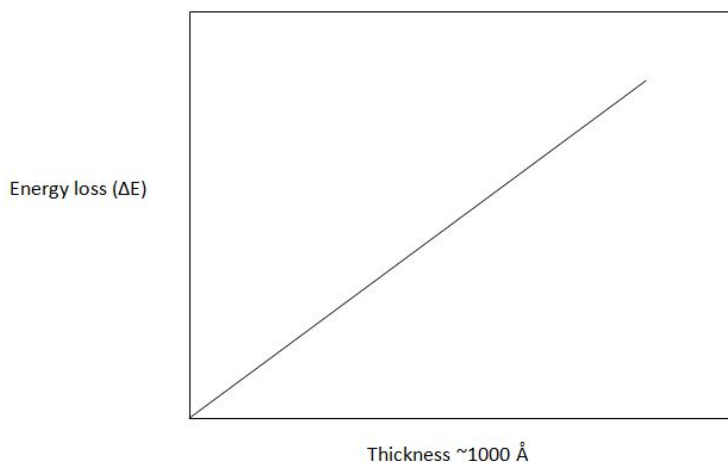


**Figure 7.3:** Variation of energy loss with the depth of the target in constant  $dE/dx$  approximation.

---

### 7.1.3 Experimental set-up

The apparatus for Rutherford backscattering analysis of thin solid surface typically consist of three components:

1. A source of helium ions.
2. An accelerator to energize the helium ions.
3. A detector to measure the energy of scattered ions.

There are two types of accelerator/ion source available. In single stage accelerator, the  $\text{He}^+$  source is placed within an insulating gas-filled tank (Figure 7.4). It is difficult to install new ion source when it is exhausted in this type of accelerator. Moreover, it is also difficult to achieve particles with energy much more than 1 MeV since it is difficult to apply high voltages in this type of system.

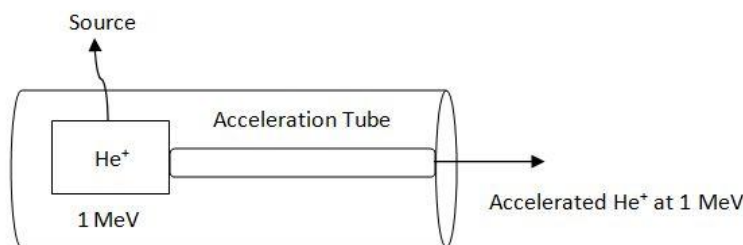


**Figure 7.4:** Schematic representation of a single stage accelerator.

Another variation is “tandem accelerator.” Here the ion source is at ground and produces negative ion. The positive terminal is located at the center of the acceleration tube (Figure 7.5). Initially the negative ion is accelerated from ground to terminal. At terminal two-electron stripping process converts the  $\text{He}^-$  to  $\text{He}^{++}$ . The positive ions are further accelerated toward ground due to columbic repulsion from positive terminal. This arrangement can achieve highly accelerated  $\text{He}^{++}$  ions ( $\sim 2.25$  MeV) with moderate voltage of 750 kV.

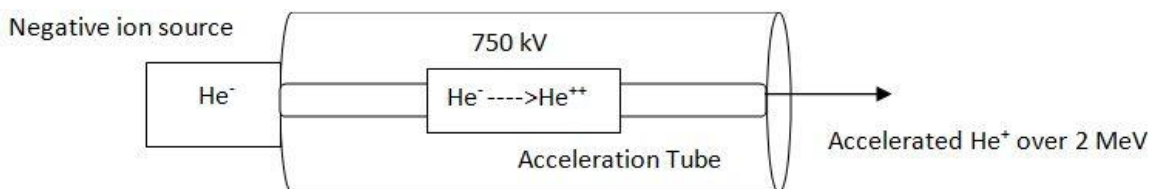


**Figure 7.5:** Schematic representation of a tandem accelerator.

Particles that are backscattered by surface atoms of the bombarded specimen are detected by a surface barrier detector. The surface barrier detector is a thin layer of p-type silicon on the n-type substrate resulting p-n junction. When the scattered ions exchange energy with the electrons on the surface of the detector upon reaching the detector, electrons get promoted from the valence band to the conduction band. Thus, each exchange of energy creates electron-hole pairs. The energy of scattered ions is detected by simply counting the number of electron-hole pairs. The energy resolution of the surface barrier detector in a standard RBS experiment is 12 - 20 keV. The surface barrier detector is generally set between  $90^\circ$  and  $170^\circ$  to the incident beam. Films are usually set normal to the incident beam. A simple layout is shown in Figure 7.6.

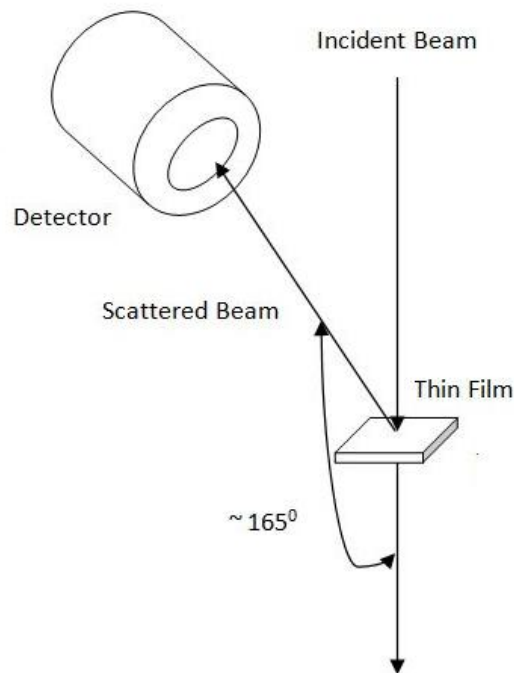


**Figure 7.6:** Schematic representation general set up where the surface barrier detector is placed at angle of  $165^\circ$  to the extrapolated incident beam.

#### 7.1.4 Depth profile analysis

As stated earlier, it is a good approximation in thin film analysis that the total energy loss  $\Delta E$  is proportional to depth  $t$ . With this approximation, we can derive the relation between energy width  $\Delta E$  of the signal from a film of thickness  $\Delta t$  as follows,

$$\Delta E = \Delta t (k \frac{dE}{dx}_{in} + \frac{1}{\cos \emptyset} \frac{dE}{dx}_{out})$$

where  $\emptyset$  = lab scattering angle.

It is worth noting that  $k$  is the kinematic factor defined in equation above and the subscripts “in” and “out” indicate the energies at which the rate of loss of energy or  $dE/dx$  is evaluated. As an example, we consider the backscattering spectrum, at scattering angle  $170^\circ$ , for 2 MeV  $\text{He}^{++}$  incidents on silicon layer deposited onto 2 mm thick niobium substrate Figure 7.7.

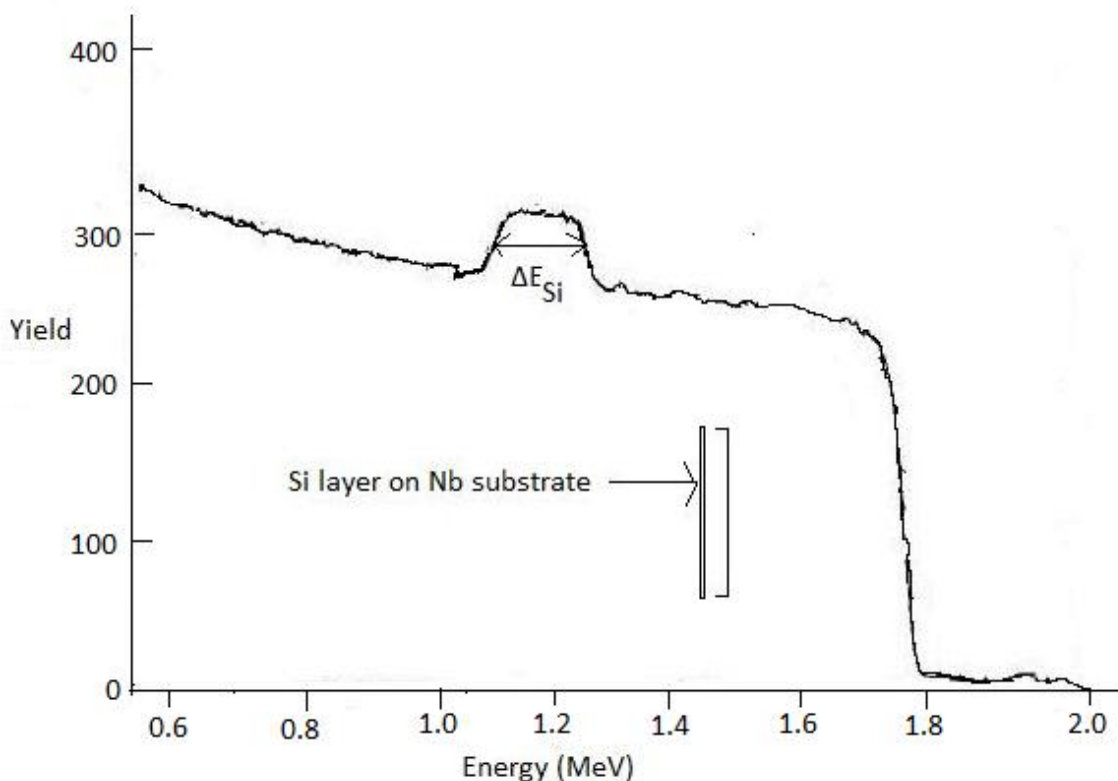


**Figure 7.7:** The backscattering spectrum for 2.0 MeV He ions incident on a silicon thin film deposited onto a niobium substrate. Adapted from P. D. Stupik, M. M. Donovan, A. R. Barron, T. R. Jervis and M. Nastasi, *Thin Solid Films*, 1992, **207**, 138.

The energy loss rate of incoming  $\text{He}^{++}$  or  $dE/dx$  along inward path in elemental Si is  $\approx 24.6 \text{ eV}/\text{\AA}$  at 2 MeV and is  $\approx 26 \text{ eV}/\text{\AA}$  for the outgoing particle at 1.12 MeV (Since  $K$  of Si is 0.56 when the scattering angle is  $170^\circ$ , energy of the outgoing particle would be equal to  $2 \times 0.56$  or 1.12 MeV). Again the value of  $\Delta E_{\text{Si}}$  is  $\approx 133.3 \text{ keV}$ . Putting the values into above equation we get

$$\begin{aligned} \Delta t &\approx 133.3 \text{ keV} / (0.56 * 24.6 \text{ eV}/\text{\AA} + 1/\cos 170^\circ * 26 \text{ eV}/\text{\AA}) \\ &= 133.3 \text{ keV} / (13.77 \text{ eV}/\text{\AA} + 29/.985 \text{ eV}/\text{\AA}) \\ &= 133.3 \text{ keV} / 40.17 \text{ eV}/\text{\AA} \\ &= 3318 \text{ \AA}. \end{aligned}$$

Hence a Si layer of ca. 3300  $\text{\AA}$  thickness has been deposited on the niobium substrate. However we need to remember that the value of  $dE/dx$  is approximated in this calculation.

### 7.1.5 Quantitative Analysis

In addition to depth profile analysis, we can study the composition of an element quantitatively by backscattering spectroscopy. The basic equation for quantitative analysis is

$$Y = \sigma \cdot \Omega \cdot Q \cdot N \Delta t$$

Where  $Y$  is the yield of scattered ions from a thin layer of thickness  $\Delta t$ ,  $Q$  is the number of incident ions and  $\Omega$  is the detector solid angle, and  $N\Delta t$  is the number of specimen atoms ( $\text{atom}/\text{cm}^2$ ). shows the RBS spectrum for a sample of silicon deposited on a niobium substrate and subjected to laser mixing. The Nb has reacted with the silicon to form a  $\text{NbSi}_2$  interphase layer. The Nb signal has broadened after the reaction as show in .

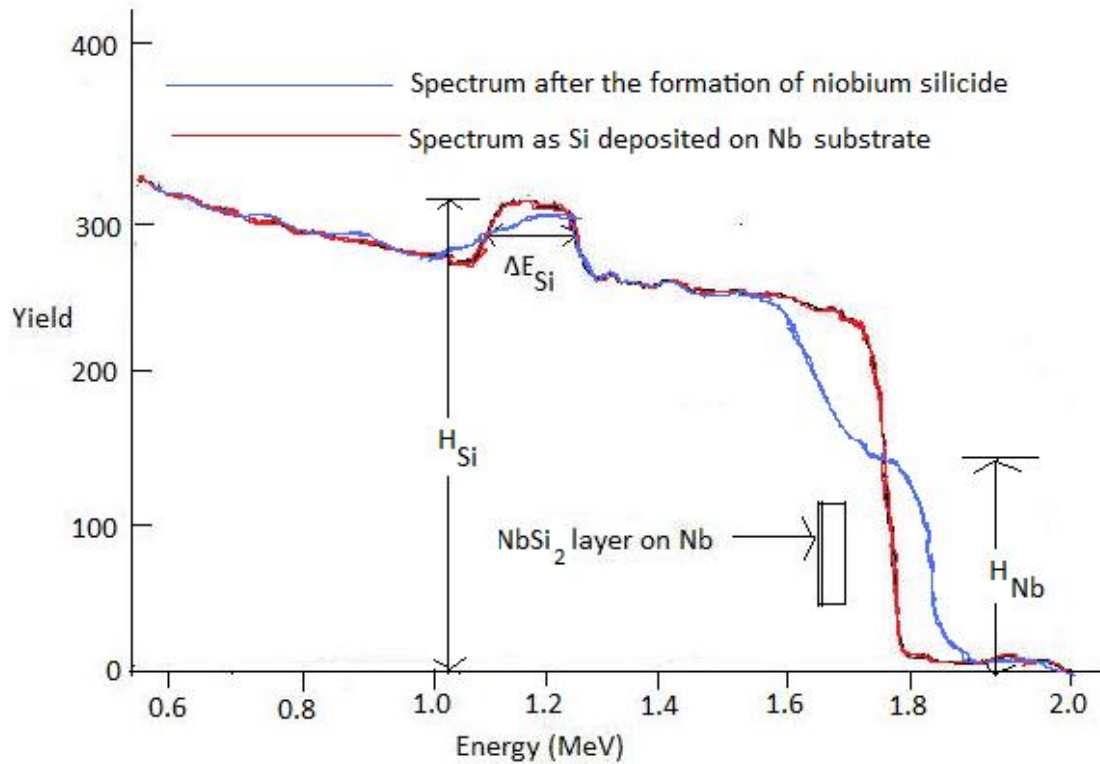


**Figure 7.8:** Backscattering spectra of Si diffused into Nb and Si as deposited on Nb substrate. Adapted from P. D. Stupik, M. M. Donovan, A. R. Barron, T. R. Jervis and M. Nastasi, *Thin Solid Films*, 1992, 207, 138.

We can use ratio of the heights  $H_{\text{Si}}/H_{\text{Nb}}$  of the backscattering spectrum after formation of  $\text{NbSi}_2$  to determine the composition of the silicide layer. The stoichiometric ratio of Nb and Si can be approximated as,

$$N_{\text{Si}}/N_{\text{Nb}} \approx [H_{\text{Si}} * \sigma_{\text{Si}}]/[H_{\text{Nb}} * \sigma_{\text{Nb}}]$$

Hence the concentration of Si and Nb can be determined if we can know the appropriate cross sections  $\sigma_{\text{Si}}$  and  $\sigma_{\text{Nb}}$ . However the yield in the backscattering spectra is better represented as the product of signal height and the energy width  $\Delta E$ . Thus stoichiometric ratio can be better approximated as

$$N_{\text{Si}}/N_{\text{Nb}} \approx [H_{\text{Si}} * \Delta E_{\text{Si}} * \sigma_{\text{Si}}]/[H_{\text{Nb}} * \Delta E_{\text{Nb}} * \sigma_{\text{Nb}}]$$

### 7.1.6 Limitations

It is of interest to understand the limitations of the backscattering technique in terms of the comparison with other thin film analysis technique such as AES, XPS and SIMS (Table 7.1). AES has better mass resolution, lateral resolution and depth resolution than RBS. But AES suffers from sputtering artifacts. Compared to RBS, SIMS has better sensitivity. RBS does not provide any chemical bonding information which we can get from XPS. Again, sputtering artifact problems are also associated in XPS. The strength of RBS lies in quantitative analysis. However, conventional RBS systems cannot analyze ultrathin films since the depth resolution is only about 10 nm using surface barrier detector.

### 7.1.7 Summary

Rutherford Backscattering analysis is a straightforward technique to determine the thickness and composition of thin films ( $< 4000 \text{ \AA}$ ). Areas that have been lately explored are the use of backscattering technique in composition determination of new superconductor oxides; analysis of lattice mismatched epitaxial layers, and as a probe of thin film morphology and surface clustering.

### 7.1.8 Bibliography

- L. C. Feldman and J. W. Mayer, *Fundamentals of Surface and Thin Film Analysis*, North Holland-Elsevier, New York (1986).
- *Ion Spectroscopies for Surface Analysis*, Ed. A. W. Czanderna and D. M. Hercules, Plenum Press (New York), 1991.
- P. D. Stupik, M. M. Donovan, A. R. Barron, T. R. Jervis, and M. Nastasi, *Thin Solid Films*, 1992, **207**, 138

## 7.2 The Application of VSI (Vertical Scanning Interferometry) to the Study of Crystal Surface Processes<sup>2</sup>

### 7.2.1 Introduction

The processes which occur at the surfaces of crystals depend on many external and internal factors such as crystal structure and composition, conditions of a medium where the crystal surface exists and others. The appearance of a crystal surface is the result of complexity of interactions between the crystal surface and the environment. The mechanisms of surface processes such as dissolution or growth are studied by the physical chemistry of surfaces. There are a lot of computational techniques which allows us to predict the changing of surface morphology of different minerals which are influenced by different conditions such as temperature, pressure, pH and chemical composition of solution reacting with the surface. For example, Monte Carlo method is widely used to simulate the dissolution or growth of crystals. However, the theoretical models of surface processes need to be verified by natural observations. We can extract a lot of useful information about the surface processes through studying the changing of crystal surface structure under influence of environmental conditions. The changes in surface structure can be studied through the observation of crystal surface topography. The topography can be directly observed macroscopically or by using microscopic techniques. Microscopic observation allows us to study even very small changes and estimate the rate of processes by observing changing the crystal surface topography in time.

Much laboratory worked under the reconstruction of surface changes and interpretation of dissolution and precipitation kinetics of crystals. Invention of AFM made possible to monitor changes of surface structure during dissolution or growth. However, to detect and quantify the results of dissolution processes or growth it is necessary to determine surface area changes over a significantly larger field of view than AFM can

<sup>2</sup>This content is available online at <http://cnx.org/content/m22326/1.4/>.

provide. More recently, vertical scanning interferometry (VSI) has been developed as new tool to distinguish and trace the reactive parts of crystal surfaces. VSI and AFM are complementary techniques and practically well suited to detect surface changes.

VSI technique provides a method for quantification of surface topography at the angstrom to nanometer level. Time-dependent VSI measurements can be used to study the surface-normal retreat across crystal and other solid surfaces during dissolution process. Therefore, VSI can be used to directly and nondirectly measure mineral dissolution rates with high precision. Analogically, VSI can be used to study kinetics of crystal growth.

### 7.2.2 Physical principles of optical interferometry

Optical interferometry allows us to make extremely accurate measurements and has been used as a laboratory technique for almost a hundred years. Thomas Young observed interference of light and measured the wavelength of light in an experiment, performed around 1801. This experiment gave an evidence of Young's arguments for the wave model for light. The discovery of interference gave a basis to development of interferometry techniques widely successfully used as in microscopic investigations, as in astronomic investigations.

The physical principles of optical interferometry exploit the wave properties of light. Light can be thought as electromagnetic wave propagating through space. If we assume that we are dealing with a linearly polarized wave propagating in a vacuum in  $z$  direction, electric field  $E$  can be represented by a sinusoidal function of distance and time.

$$E(x, y, z, t) = a \cos [2\pi (vt - z/\lambda)] \quad (7.1)$$

Where  $a$  is the amplitude of the light wave,  $v$  is the frequency, and  $\lambda$  is its wavelength. The term within the square brackets is called the phase of the wave. Let's rewrite this equation in more compact form,

$$E(x, y, z, t) = a \cos [\omega t - kz] \quad (7.2)$$

where  $\omega = 2\pi v$  is the circular frequency, and  $k = 2\pi/\lambda$  is the propagation constant. Let's also transform this second equation into a complex exponential form,

$$E(x, y, z, t) = \text{Re}\{a \exp(i\varphi) \exp(i\omega t)\} = \text{Re}\{A \exp(i\omega t)\} \quad (7.3)$$

where  $\varphi = 2\pi z/\lambda$  and  $A = \exp(-i\varphi)$  is known as the complex amplitude. If  $n$  is a refractive index of a medium where the light propagates, the light wave traverses a distance  $d$  in such a medium. The equivalent optical path in this case is

$$p = n \cdot d \quad (7.4)$$

When two light waves are superposed, the result intensity at any point depends on whether reinforce or cancel each other (Figure 7.9). This is well known phenomenon of interference. We will assume that two waves are propagating in the same direction and are polarized with their field vectors in the same plane. We will also assume that they have the same frequency. The complex amplitude at any point in the interference pattern is then the sum of the complex amplitudes of the two waves, so that we can write,

$$A = A_1 + A_2 \quad (7.5)$$

where  $A_1 = a_1 \exp(-i\varphi_1)$  and  $A_2 = a_2 \exp(-i\varphi_2)$  are the complex amplitudes of two waves. The resultant intensity is, therefore,

$$I = |A|^2 = I_1 + I_2 + 2(I_1 I_2)^{1/2} \cos \Delta\varphi \quad (7.6)$$

where  $I_1$  and  $I_2$  are the intensities of two waves acting separately, and  $\Delta\varphi = \varphi_1 - \varphi_2$  is the phase difference between them. If the two waves are derived from a common source, the phase difference corresponds to an optical path difference,

$$\Delta p = (\lambda/2\pi) \Delta\varphi \quad (7.7)$$

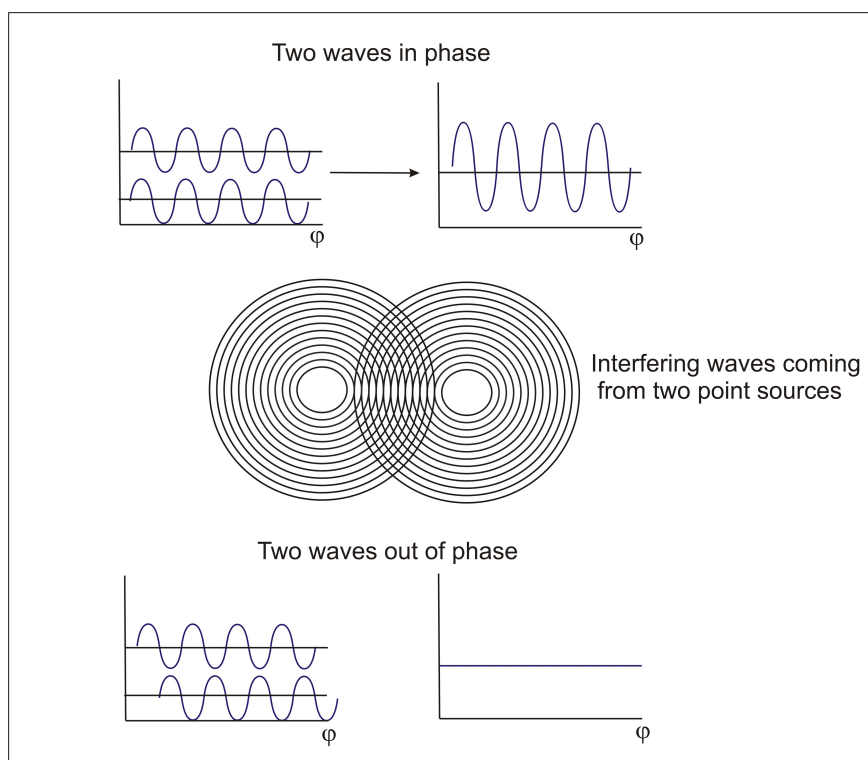


**Figure 7.9:** The scheme of interferometric wave interaction when two waves interact with each other, the amplitude of resulting wave will increase or decrease. The value of this amplitude depends on phase difference between two original waves.

If  $\Delta\varphi$ , the phase difference between the beams, varies linearly across the field of view, the intensity varies sinusoidally, giving rise to alternating light and dark bands or fringes (Figure 7.9). The intensity in an interference pattern has its maximum value

$$I_{\max} = I_1 + I_2 + 2(I_1 I_2)^{1/2} \quad (7.8)$$

when  $\Delta\varphi = 2m\pi$ , where  $m$  is an integer and its minimum value

$$I_{\min} = I_1 + I_2 - 2(I_1 I_2)^{1/2} \quad (7.9)$$

when  $\Delta\varphi = (2m + 1)\pi$ .

The principle of interferometry is widely used to develop many types of interferometric set ups. One of the earliest set ups is Michelson interferometry. The idea of this interferometry is quite simple: interference

fringes are produced by splitting a beam of monochromatic light so that one beam strikes a fixed mirror and the other a movable mirror. An interference pattern results when the reflected beams are brought back together. The Michelson interferometric scheme is shown in Figure 7.10.

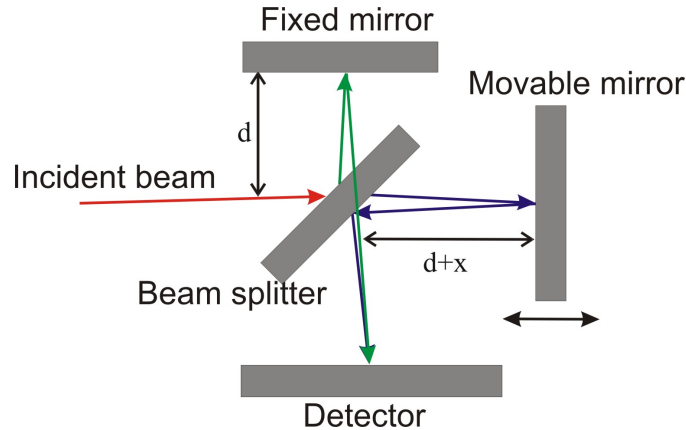


**Figure 7.10:** Schematic representation of a Michelson interferometry set-up.

The difference of path lengths between two beams is  $2x$  because beams traverse the designated distances twice. The interference occurs when the path difference is equal to integer numbers of wavelengths,

$$\Delta p = 2x = m\lambda, m = 0, \pm 1, \pm 2 \dots \quad (7.10)$$

Modern interferometric systems are more complicated. Using special phase-measurement techniques they are capable of performing much more accurate height measurements than can be obtained just by directly looking at the interference fringes and measuring how they depart from being straight and equally spaced. Typically an interferometric system consists of a light source, beamsplitter, objective system, system of registration of signals, and transformation into digital format and computer which processes the data. Vertical scanning interferometry contains all these parts. Figure 7.11 shows a configuration of VSI interferometric system.

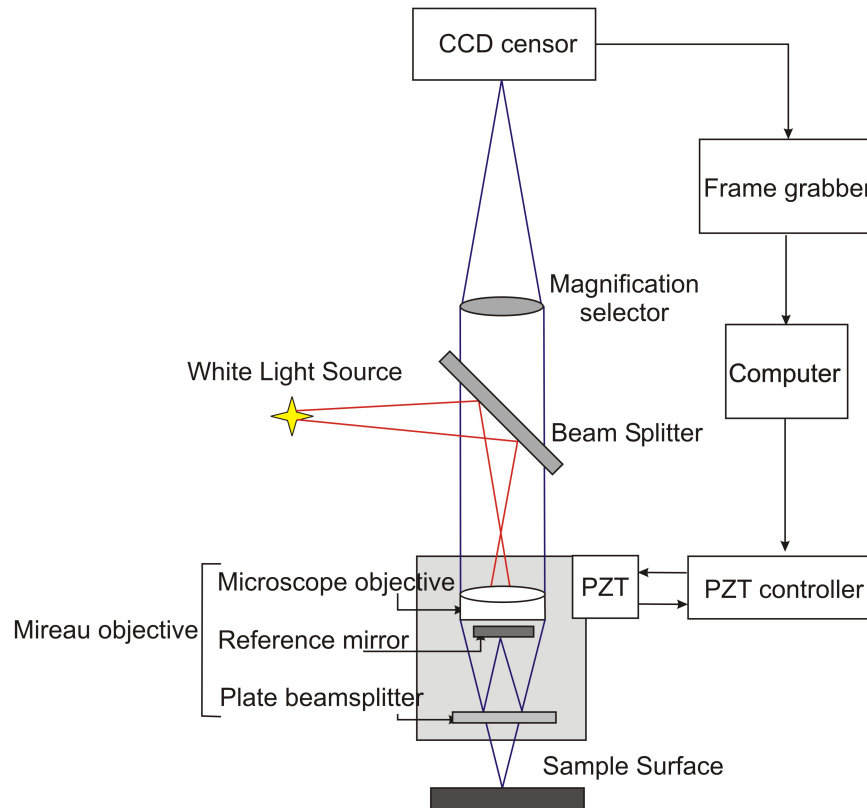


**Figure 7.11:** Schematic representation of the Vertical scanning interferometry (VSI) system.

Many of modern interferometric systems use Mirau objective in their constructions. Mireau objective is based on a Michelson interferometer. This objective consists of a lens, a reference mirror and a beamsplitter. The idea of getting interfering beams is simple: two beams (red lines) travel along the optical axis. Then they are reflected from the reference surface and the sample surface respectively (blue lines). After this these beams are recombined to interfere with each other. An illumination or light source system is used to direct light onto a sample surface through a cube beam splitter and the Mireau objective. The sample surface within the field of view of the objective is uniformly illuminated by those beams with different incidence angles. Any point on the sample surface can reflect those incident beams in the form of divergent cone. Similarly, the point on the reference symmetrical with that on the sample surface also reflects those illuminated beams in the same form.

The Mireau objective directs the beams reflected of the reference and the sample surface onto a CCD (charge-coupled device) sensor through a tube lens. The CCD sensor is an analog shift register that enables the transportation of analog signals (electric charges) through successive stages (capacitors), controlled by a clock signal. The resulting interference fringe pattern is detected by CCD sensor and the corresponding signal is digitized by a frame grabber for further processing with a computer.

The distance between a minimum and a maximum of the interferogram produced by two beams reflected from the reference and sample surface is known. That is, exactly half the wavelength of the light source. Therefore, with a simple interferogram the vertical resolution of the technique would be also limited to  $\lambda/2$ . If we will use a laser light as a light source with a wavelength of 300 nm the resolution would be only 150

nm. This resolution is not good enough for a detailed near-atomic scale investigation of crystal surfaces. Fortunately, the vertical resolution of the technique can be improved significantly by moving either the reference or the sample by a fraction of the wavelength of the light. In this way, several interferograms are produced. Then they are all overlaid, and their phase shifts compared by the computer software Figure 7.12. This method is widely known as phase shift interferometry (PSI).

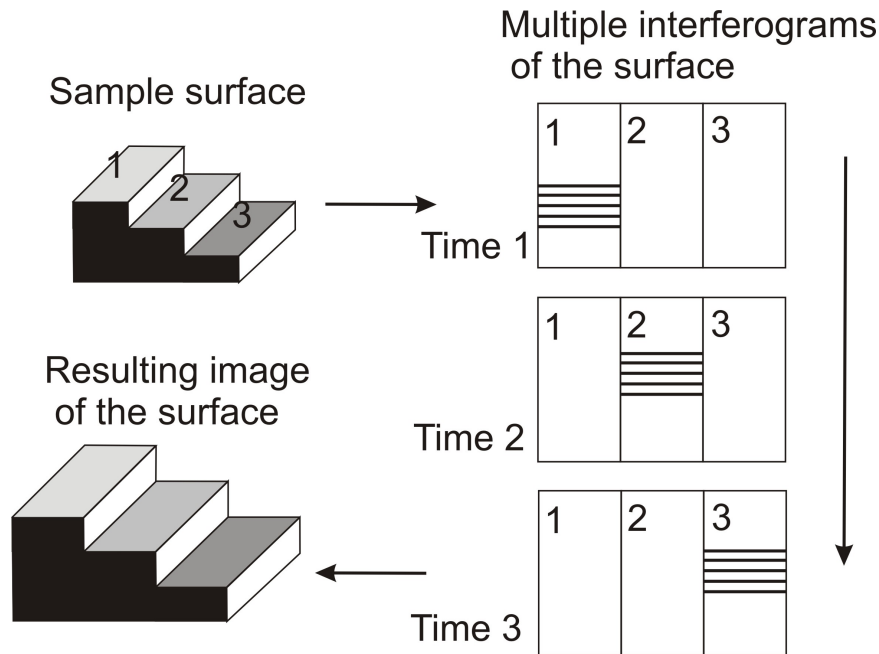


**Figure 7.12:** Sketch illustrating phase-shift technology. The sample is continuously moved along the vertical axes in order to scan surface topography. All interferograms are automatically overlaid using computer software.

Most optical testing interferometers now use phase-shifting techniques not only because of high resolution but also because phase-shifting is a high accuracy rapid way of getting the interferogram information into the computer. Also usage of this technique makes the inherent noise in the data taking process very low. As the result in a good environment angstrom or sub-angstrom surface height measurements can be performed. As it was said above, in phase-shifting interferometry the phase difference between the interfering beams is changed at a constant rate as the detector is read out. Once the phase is determined across the interference field, the corresponding height distribution on the sample surface can be determined. The phase distribution  $\phi(x, y)$  is recorded by using the CCD camera.

Let's assign  $A(x, y)$ ,  $B(x, y)$ ,  $C(x, y)$  and  $D(x, y)$  to the resulting interference light intensities which are corresponded to phase-shifting steps of  $0$ ,  $\pi/2$ ,  $\pi$  and  $3\pi/2$ . These intensities can be obtained by moving the reference mirror through displacements of  $\lambda/8$ ,  $\lambda/4$  and  $3\lambda/8$ , respectively. The equations for the resulting intensities would be:

$$A(x, y) = I_1(x, y) + I_2(x, y) \cos \alpha(x, y) \quad (7.11)$$

$$B(x, y) = I_1(x, y) - I_2(x, y) \sin \alpha(x, y) \quad (7.12)$$

$$C(x, y) = I_1(x, y) - I_2(x, y) \cos\alpha(x, y) \quad (7.13)$$

$$D(x, y) = I_1(x, y) + I_2(x, y) \sin\alpha(x, y) \quad (7.14)$$

where  $I_1(x, y)$  and  $I_2(x, y)$  are two overlapping beams from two symmetric points on the test surface and the reference respectively. Solving equations (7.11)–(7.14), the phase map  $\phi(x, y)$  of a sample surface will be given by the relation:

$$\varphi(x, y) = \frac{B(x, y) - D(x, y)}{A(x, y) - C(x, y)} \quad (7.15)$$

Once the phase is determined across the interference field pixel by pixel on a two-dimensional CCD array, the local height distribution/contour,  $h(x, y)$ , on the test surface is given by

$$h(x, y) = \frac{\lambda}{4\pi} \varphi(x, y) \quad (7.16)$$

Normally the resulted fringe can be in the form of a linear fringe pattern by adjusting the relative position between the reference mirror and sample surfaces. Hence any distorted interference fringe would indicate a local profile/contour of the test surface.

It is important to note that the Mireau objective is mounted on a capacitive closed-loop controlled PZT (piezoelectric actuator) as to enable phase shifting to be accurately implemented. The PZT is based on piezoelectric effect referred to the electric potential generated by applying pressure to piezoelectric material. This type of materials is used to convert electrical energy to mechanical energy and vice-versa. The precise motion that results when an electric potential is applied to a piezoelectric material has an importance for nanopositioning. Actuators using the piezo effect have been commercially available for 35 years and in that time have transformed the world of precision positioning and motion control.

Vertical scanning interferometer also has another name; white-light interferometry (WLI) because of using the white light as a source of light. With this type of source a separate fringe system is produced for each wavelength, and the resultant intensity at any point of examined surface is obtained by summing these individual patterns. Due to the broad bandwidth of the source the coherent length  $L$  of the source is short:

$$L = \frac{\lambda^2}{n\Delta\lambda} \quad (7.17)$$

where  $\lambda$  is the center wavelength,  $n$  is the refractive index of the medium,  $\Delta\lambda$  is the spectral width of the source. In this way good contrast fringes can be obtained only when the lengths of interfering beams pathways are closed to each other. If we will vary the length of a pathway of a beam reflected from sample, the height of a sample can be determined by looking at the position for which a fringe contrast is a maximum. In this case interference pattern exist only over a very shallow depth of the surface. When we vary a pathway of sample-reflected beam we also move the sample in a vertical direction in order to get the phase at which maximum intensity of fringes will be achieved. This phase will be converted in height of a point at the sample surface.

The combination of phase shift technology with white-light source provides a very powerful tool to measure the topography of quite rough surfaces with the amplitude in heights about and the precision up to 1-2 nm. Through a developed software package for quantitatively evaluating the resulting interferogram, the proposed system can retrieve the surface profile and topography of the sample objects Figure 7.13.

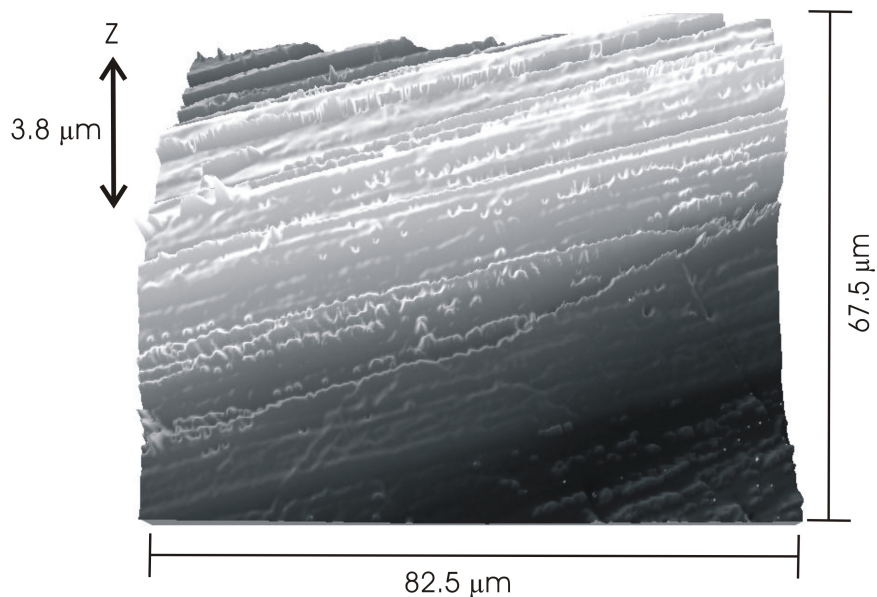


**Figure 7.13:** Example of muscovite surface topography, obtained by using VSI- 50x objective.

---

### 7.2.3 A comparison of common methods to determine surface topography: SEM, AFM and VSI

Except the interferometric methods described above, there are a several other microscopic techniques for studying crystal surface topography. The most common are scanning electron microscopy (SEM) and atomic force microscopy (AFM). All these techniques are used to obtain information about the surface structure. However they differ from each other by the physical principles on which they based.

#### 7.2.3.1 Scanning electron microscopy

SEM allows us to obtain images of surface topography with the resolution much higher than the conventional light microscopes do. Also it is able to provide information about other surface characteristics such as chemical composition, electrical conductivity etc, see Figure 7.14. All types of data are generated by the reflecting of accelerated electron beams from the sample surface. When electrons strike the sample surface, they lose their energy by repeated random scattering and adsorption within an outer layer into the depth varying from 100 nm to 5 microns.

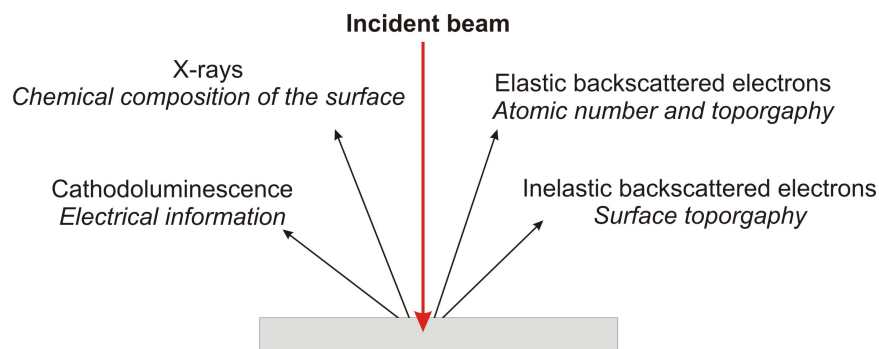


**Figure 7.14:** Scheme of electron beam-sample interaction at SEM analysis

The thickness of this outer layer also known as interactive layer depends on energy of electrons in the beam, composition and density of a sample. Result of the interaction between electron beam and the surface provides several types of signals. The main type is secondary or inelastic scattered electrons. They are produced as a result of interaction between the beam of electrons and weakly bound electrons in the conduction band of the sample. Secondary electrons are ejected from the  $k$ -orbitals of atoms within the surface layer of thickness about a few nanometers. This is because secondary electrons are low energy electrons ( $<50$  eV), so only those formed within the first few nanometers of the sample surface have enough energy to escape and be detected. Secondary backscattered electrons provide the most common signal to investigate surface topography with lateral resolution up to 0.4 - 0.7 nm.

High energy beam electrons are elastic scattered back from the surface. This type of signal gives information about chemical composition of the surface because the energy of backscattered electrons depends on the weight of atoms within the interaction layer. Also this type of electrons can form secondary electrons and escape from the surface or travel farther into the sample than the secondary. The SEM image formed is the result of the intensity of the secondary electron emission from the sample at each  $x,y$  data point during the scanning of the surface.

### 7.2.3.2 Atomic force microscopy

AFM is a very popular tool to study surface dissolution. AFM set up consists of scanning a sharp tip on the end of a flexible cantilever which moves across a sample surface. The tips typically have an end radius of 2 to 20 nm, depending on tip type. When the tip touches the surface the forces of these interactions lead to deflection of a cantilever. The interaction between tip and sample surface involves mechanical contact forces, van der Waals forces, capillary forces, chemical bonding, electrostatic forces, magnetic forces etc. The deflection of a cantilever is usually measured by reflecting a laser beam off the back of the cantilever into a split photodiode detector. A schematic drawing of AFM can be seen in Figure 7.15. The two most commonly used modes of operation are contact mode AFM and tapping mode AFM, which are conducted in air or liquid environments.

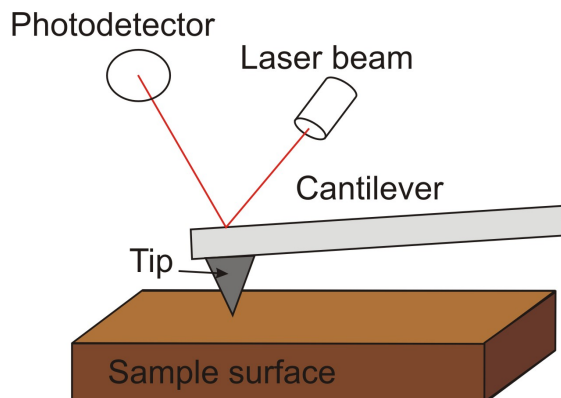


**Figure 7.15:** Schematic drawing of an AFM apparatus.

Working under the contact mode AFM scans the sample while monitoring the change in cantilever deflection with the split photodiode detector. Loop maintains a constant cantilever reflection by vertically moving the scanner to get a constant signal. The distance which the scanner goes by moving vertically at each x,y data point is stored by the computer to form the topographic image of the sample surface. Working under the tapping mode AFM oscillates the cantilever at its resonance frequency (typically  $\sim 300$  kHz) and lightly “taps” the tip on the surface during scanning. The electrostatic forces increase when tip gets close to the sample surface, therefore the amplitude of the oscillation decreases. The laser deflection method is used to detect the amplitude of cantilever oscillation. Similar to the contact mode, feedback loop maintains a constant oscillation amplitude by moving the scanner vertically at every x,y data point. Recording this movement forms the topographical image. The advantage of tapping mode over contact mode is that it eliminates the lateral, shear forces present in contact mode. This enables tapping mode to image soft, fragile, and adhesive surfaces without damaging them while work under contact mode allows the damage to occur.

### 7.2.3.3 Comparison of techniques

All techniques described above are widely used in studying of surface nano- and micromorphology. However, each method has its own limitations and the proper choice of analytical technique depends on features of analyzed surface and primary goals of research.

All these techniques are capable to obtain an image of a sample surface with quite good resolution. The lateral resolution of VSI is much less, then for other techniques: 150 nm for VSI and 0.5 nm for AFM and SEM. Vertical resolution of AFM (0.5 Å) is better then for VSI (1 - 2 nm), however VSI is capable to measure a high vertical range of heights (1 mm) which makes possible to study even very rough surfaces. On the contrary, AFM allows us to measure only quite smooth surfaces because of its relatively small vertical scan range (7  $\mu\text{m}$ ). SEM has less resolution, than AFM because it requires coating of a conductive material with the thickness within several nm.

The significant advantage of VSI is that it can provide a large field of view (845  $\times$  630  $\mu\text{m}$  for 10x objective) of tested surfaces. Recent studies of surface roughness characteristics showed that the surface roughness parameters increase with the increasing field of view until a critical size of 250,000  $\mu\text{m}$  is reached. This value is larger then the maximum field of view produced by AFM (100  $\times$  100  $\mu\text{m}$ ) but can be easily obtained by VSI. SEM is also capable to produce images with large field of view. However, SEM is able to provide only 2D images from one scan while AFM and VSI let us to obtain 3D images. It makes quantitative

analysis of surface topography more complicated, for example, topography of membranes is studied by cross section and top view images.

	VSI	AFM	SEM
Lateral resolution	0.5-1.2 $\mu\text{m}$	0.5 nm	0.5-1 nm
Vertical resolution	2 nm	0.5 $\text{\AA}$	Only 2D images
Field of view	845 $\times$ 630 $\mu\text{m}$ (10x objective)	100 $\times$ 100 $\mu\text{m}$	1-2 mm
Vertical range of scan	1 mm	10 $\mu\text{m}$	-
Preparation of a sample	-	-	Required coating of a conducted material
Required environment	Air	Air, liquid	Vacuum

**Table 7.2:** A comparison of VSI sample and resolution with AFM and SEM.

#### 7.2.4 The experimental studying of surface processes using microscopic techniques

The limitations of each technique described above are critically important to choose appropriate technique for studying surface processes. Let's explore application of these techniques to study dissolution of crystals.

When crystalline matter dissolves the changes of the crystal surface topography can be observed by using microscopic techniques. If we will apply an unreactive mask (silicon for example) on crystal surface and place a crystalline sample into the experiment reactor then we get two types of surfaces: dissolving and remaining the same or unreacted. After some period of time the crystal surface starts to dissolve and change its z-level. In order to study these changes *ex situ* we can pull out a sample from the reaction cell then remove a mask and measure the average height difference  $\Delta \bar{h}$  between the unreacted and dissolved areas. The average heights of dissolved and unreacted areas are obtained through digital processing of data obtained by microscopes. The velocity of normal surface retreat  $v_{\text{SNR}}$  during the time interval  $\Delta t$  is defined as

$$v_{\text{SNR}} = \frac{\Delta \bar{h}}{\Delta t}$$

Dividing this velocity by the molar volume  $\bar{V}$  ( $\text{cm}^3/\text{mol}$ ) gives a global dissolution rate in the familiar units of moles per unit area per unit time:

$$R = \frac{v_{\text{SNR}}}{\bar{V}} \quad (7.18)$$

This method allows us to obtain experimental values of dissolution rates just by precise measuring of average surface heights. Moreover, using this method we can measure local dissolution rates at etch pits by monitoring changes in the volume and density of etch pits across the surface over time. VSI technique is capable to perform these measurements because of large vertical range of scanning. In order to get precise values of rates which are not depend on observing place of crystal surface we need to measure enough large areas. VSI technique provides data from areas which are large enough to study surfaces with heterogeneous dissolution dynamics and obtain average dissolution rates. Therefore, VSI makes possible to measure rates of normal surface retreat during the dissolution and observe formation, growth and distribution of etch pits on the surface.

However, if the mechanism of dissolution is controlled by dynamics of atomic steps and kink sites within a smooth atomic surface area, the observation of the dissolution process need to use a more precise technique. AFM is capable to provide information about changes in step morphology *in situ* when the dissolution

occurs. For example, immediate response of the dissolved surface to the changing of environmental conditions (concentrations of ions in the solution, pH etc.) can be studied by using AFM.

SEM is also used to examine micro and nanotexture of solid surfaces and study dissolution processes. This method allows us to observe large areas of crystal surface with high resolution which makes possible to measure a high variety of surfaces. The significant disadvantage of this method is the requirement to cover examine sample by conductive substance which limits the resolution of SEM. The other disadvantage of SEM is that the analysis is conducted in vacuum. Recent technique, environmental SEM or ESEM overcomes these requirements and makes possible even examine liquids and biological materials. The third disadvantage of this technique is that it produces only 2D images. This creates some difficulties to measure  $\Delta\bar{h}$  within the dissolving area. One of advantages of this technique is that it is able to measure not only surface topography but also chemical composition and other surface characteristics of the surface. This fact is used to monitor changing in chemical composition during the dissolution.

### 7.2.5 Bibliography

- A. C. Lasaga, *Kinetic Theory in the Earth Sciences*. Princeton Univ. Press, Princeton, NJ (1998).
- A. Luttge, E. V. Bolton, and A. C. Lasaga A.C., *Am. J. Sci.*, 1999, **299**, 652.
- D. Kaczmarek, *Vacuum*, 2001, **62**, 303.
- P. Hariharan. *Optical interferometry*, Second edition, Academic press (2003) ISBN 0-12-311630-9.
- A. Luttge and P. G. Conrad, *Appl. Environ. Microbiol.*, 2004, **70**, 1627.
- A. C. Lasaga and A. Luttge, *American Mineralogist*, 2004, **89**, 527.
- K. J. Davis and A. Luttge, *Am. J. Sci.*, 2005, **305**, 727.
- S. H. Wang and Tay, *Meas. Sci. Technol.*, 2006, **17**, 617.
- A. Luttge and R. S. Arvidson, in *Kinetics of water-rock interaction*, Ed. S. Brantley, J. Kubicki, and A. White, Springer (2007).
- L. Zhang and A. Luttge, *American Mineralogist*, 2007, **92**, 1316.
- C. Fischer A. and Luttge, *Am. J. Sci.*, 2007, **307**, 955.
- Y. Wyart, G. Georges, C. Deumie, C. Amra, and P. Moulina, *J. Membrane Sci.*, 2008, **315**, 82.
- T. C. Vaimakis, E. D. Economou, and C. C. Trapalis, *J. Therm. Anal. Cal.*, 2008, **92**, 783.

## 7.3 Atomic Force Microscopy<sup>3</sup>

### 7.3.1 Introduction

Atomic force microscopy (AFM) is a high-resolution form of scanning probe microscopy, also known as scanning force microscopy (SFM). The instrument uses a cantilever with a sharp tip at the end to scan over the sample surface (Figure 7.16). As the probe scans over the sample surface, attractive or repulsive forces between the tip and sample, usually in the form of van der Waal forces but also can be a number of others such as electrostatic and hydrophobic/hydrophilic, cause a deflection of the cantilever. The deflection is measured by a laser (Figure 7.16) which is reflected off the cantilever into photodiodes. As one of the photodiodes collects more light, it creates an output signal that is processed and provides information about the vertical bending of the cantilever. This data is then sent to a scanner that controls the height of the probe as it moves across the surface. The variance in height applied by the scanner can then be used to produce a three-dimensional topographical representation of the sample.

<sup>3</sup>This content is available online at <<http://cnx.org/content/m34664/1.1/>>.

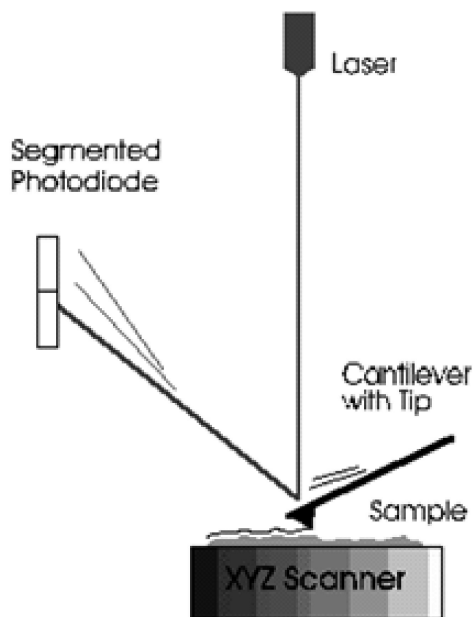


**Figure 7.16:** Simple schematic of atomic force microscope (AFM) apparatus. Adapted from H. G. Hansma, Department of Physics, University of California, Santa Barbara.

---

## 7.3.2 Modes of operation

### 7.3.2.1 Contact mode

The contact mode method utilizes a constant force for tip-sample interactions by maintaining a constant tip deflection (Figure 7.17). The tip communicates the nature of the interactions that the probe is having at the surface via feedback loops and the scanner moves the entire probe in order to maintain the original deflection of the cantilever. The constant force is calculated and maintained by using Hooke's Law, (7.19). This equation relates the force ( $F$ ), spring constant ( $k$ ), and cantilever deflection ( $x$ ). Force constants typically range from 0.01 to 1.0 N/m. Contact mode usually has the fastest scanning times but can deform the sample surface. It is also only the only mode that can attain "atomic resolution."

$$F = -kx \tag{7.19}$$



**Figure 7.17:** Schematic diagram of probe and surface interaction in contact mode.

---

### 7.3.2.2 Tapping mode

In the tapping mode the cantilever is externally oscillated at its fundamental resonance frequency (Figure 7.18). A piezoelectric on top of the cantilever is used to adjust the amplitude of oscillation as the probe scans across the surface. The deviations in the oscillation frequency or amplitude due to interactions between the probe and surface are measured, and provide information about the surface or types of material present in the sample. This method is gentler than contact AFM since the tip is not dragged across the surface, but it does require longer scanning times. It also tends to provide higher lateral resolution than contact AFM.

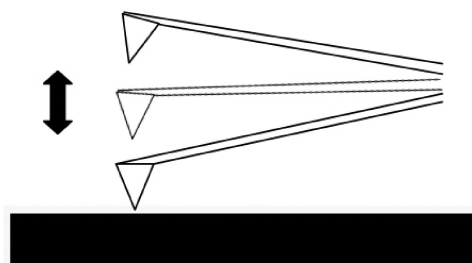


**Figure 7.18:** Diagram of probe and surface interaction in tapping mode.

---

### 7.3.2.3 Noncontact mode

For noncontact mode the cantilever is oscillated just above its resonance frequency and this frequency is decreased as the tip approaches the surface and experiences the forces associated with the material (Figure 7.19). The average tip-to-sample distance is measured as the oscillation frequency or amplitude is kept constant, which then can be used to image the surface. This method exerts very little force on the sample, which extends the lifetime of the tip. However, it usually does not provide very good resolution unless placed under a strong vacuum.

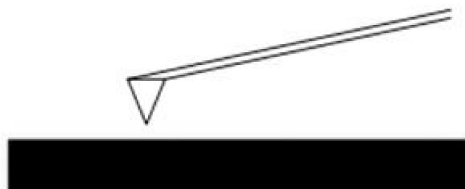


**Figure 7.19:** Diagram of probe and surface interaction in noncontact mode.

---

### 7.3.3 Experimental limitations

A common problem seen in AFM images is the presence of artifacts which are distortions of the actual topography, usually either due to issues with the probe, scanner, or image processing. The AFM scans slowly which makes it more susceptible to external temperature fluctuations leading to thermal drift. This leads to artifacts and inaccurate distances between topographical features.

It is also important to consider that the tip is not perfectly sharp and therefore may not provide the best aspect ratio, which leads to a convolution of the true topography. This leads to features appearing too large or too small since the width of the probe cannot precisely move around the particles and holes on the surface. It is for this reason that tips with smaller radii of curvature provide better resolution in imaging. The tip can also produce false images and poorly contrasted images if it is blunt or broken.

The movement of particles on the surface due to the movement of the cantilever can cause noise, which forms streaks or bands in the image. Artifacts can also be made by the tip being of inadequate proportions compared to the surface being scanned. It is for this reason that it is important to use the ideal probe for the particular application.

### 7.3.4 Sample size and preparation

The sample size varies with the instrument but a typical size is 8 mm by 8 mm with a typical height of 1 mm. Solid samples present a problem for AFM since the tip can shift the material as it scans the surface. Solutions or dispersions are best for applying as uniform of a layer of material as possible in order to get the most accurate value of particles' heights. This is usually done by spin-coating the solution onto freshly cleaved mica which allows the particles to stick to the surface once it has dried.

### 7.3.5 Applications of AFM

AFM is particularly versatile in its applications since it can be used in ambient temperatures and many different environments. It can be used in many different areas to analyze different kinds of samples such as semiconductors, polymers, nanoparticles, biotechnology, and cells amongst others. The most common application of AFM is for morphological studies in order to attain an understanding of the topography of the sample. Since it is common for the material to be in solution, AFM can also give the user an idea of the ability of the material to be dispersed as well as the homogeneity of the particles within that dispersion. It also can provide a lot of information about the particles being studied such as particle size, surface area, electrical properties, and chemical composition. Certain tips are capable of determining the principal mechanical, magnetic, and electrical properties of the material. For example, in magnetic force microscopy (MFM) the probe has a magnetic coating that senses magnetic, electrostatic, and atomic interactions with the surface.

This type of scanning can be performed in static or dynamic mode and depicts the magnetic structure of the surface.

### 7.3.5.1 AFM of carbon nanotubes

Atomic force microscopy is usually used to study the topographical morphology of these materials. By measuring the thickness of the material it is possible to determine if bundling occurred and to what degree. Other dimensions of the sample can also be measured such as the length and width of the tubes or bundles. It is also possible to detect impurities, functional groups (Figure 7.20), or remaining catalyst by studying the images. Various methods of producing nanotubes have been found and each demonstrates a slightly different profile of homogeneity and purity. These impurities can be carbon coated metal, amorphous carbon, or other allotropes of carbon such as fullerenes and graphite. These facts can be utilized to compare the purity and homogeneity of the samples made from different processes, as well as monitor these characteristics as different steps or reactions are performed on the material. The distance between the tip and the surface has proven itself to be an important parameter in noncontact mode AFM and has shown that if the tip is moved past the threshold distance, approximately  $30\ \mu\text{m}$ , it can move or damage the nanotubes. If this occurs, a useful characterization cannot be performed due to these distortions of the image.

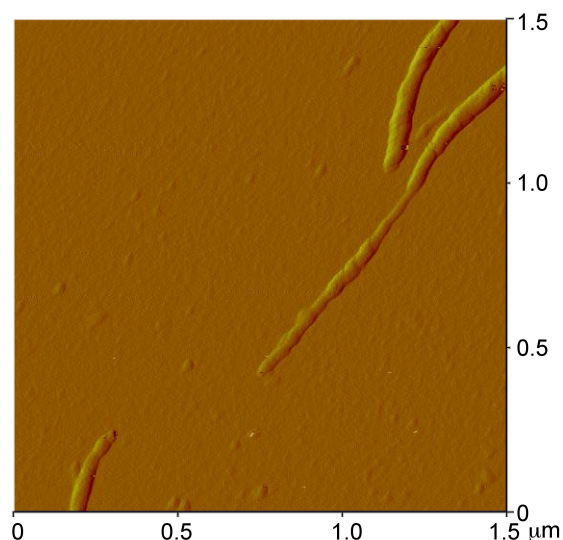


**Figure 7.20:** AFM image of a polyethyleneimine-functionalized single walled carbon nanotube (PEI-SWNT) showing the presence of PEI “globules” on the SWNT. Adapted from E. P. Dillon, C. A. Crouse, and A. R. Barron, *ACS Nano*, 2008, **2**, 156.

---

### 7.3.5.2 AFM of fullerenes

Atomic force microscopy is best applied to aggregates of fullerenes rather than individual ones. While the AFM can accurately perform height analysis of individual fullerene molecules, it has poor lateral resolution and it is difficult to accurately depict the width of an individual molecule. Another common issue that arises with contact AFM and fullerene deposited films is that the tip shifts clusters of fullerenes which can lead to discontinuities in sample images.

### 7.3.6 Bibliography

- R. Anderson and A. R. Barron, *J. Am. Chem. Soc.*, 2005, **127**, 10458.
- M. Bellucci, G. Gaggiotti, M. Marchetti, F. Micciulla, R. Mucciato, and M. Regi, *J. Physics: Conference Series*, 2007, **61**, 99.
- I. I. Bobrinetskii, V. N. Kukin, V. K. Nevolin, and M. M. Simunin. *Semiconductor*, 2008, **42**, 1496.
- S. H. Cohen and M. L. Lightbody. *Atomic Force Microscopy/Scanning Tunneling Microscopy 2*. Plenum, New York (1997).
- E. P. Dillon, C. A. Crouse, and A. R. Barron, *ACS Nano*, 2008, **2**, 156.
- C. Gu, C. Ray, S. Guo, and B. B. Akhremitchev, *J. Phys. Chem.*, 2007, **111**, 12898.
- G. Kaupp, *Atomic Force Microscopy, Scanning Nearfield Optical Microscopy and Nanoscratching: Application to Rough and Natural Surfaces*. Springer-Verlag, Berlin (2006).
- S. Morita, R. Wiesendanger, E. Meyer, and F. J. Giessibl. *Noncontact Atomic Force Microscopy*. Springer, Berlin (2002).

